European Journal of Medicinal Chemistry 156 (2018) 598–617

Contents lists available at ScienceDirect

European Journal of Medicinal Chemistry

journal homepage: http://www.elsevier.com/locate/ejmech

Research paper

Multi-target-directed ligands for treating Alzheimer's disease: Butyrylcholinesterase inhibitors displaying antioxidant and neuroprotective activities

Damijan Knez [a], Nicolas Coquelle [b, c, d, 1], Anja Pišlar [a], Simon Žakelj [a], Marko Jukič [a], Matej Sova [a], Janez Mravljak [a], Florian Nachon [e], Xavier Brazzolotto [e], Janko Kos [a], Jacques-Philippe Colletier [b, c, d], Stanislav Gobec [a, *]

[a] Faculty of Pharmacy, University of Ljubljana, Aškerčeva 7, 1000, Ljubljana, Slovenia
[b] University Grenoble Alpes, IBS, F-38044, Grenoble, France
[c] CNRS, IBS, F-38044, Grenoble, France
[d] CEA, IBS, F-38044, Grenoble, France
[e] Institut de Recherche Biomédicale des Armées, 91223, Brétigny sur Orge, France

ARTICLE INFO

Article history:
Received 15 June 2018
Received in revised form
11 July 2018
Accepted 12 July 2018

Keywords:
Alzheimer's disease
Butyrylcholinesterase
Multi-target-directed ligands
Antioxidant
8-hydroxyquinoline

ABSTRACT

The limited clinical efficacy of current symptomatic treatment and minute effect on progression of Alzheimer's disease has shifted the research focus from single targets towards multi-target-directed ligands. Here, a potent selective inhibitor of human butyrylcholinesterase was used as the starting point to develop a new series of multifunctional ligands. A focused library of derivatives was designed and synthesised that showed both butyrylcholinesterase inhibition and good antioxidant activity as determined by the DPPH assay. The crystal structure of compound **11** in complex with butyrylcholinesterase revealed the molecular basis for its low nanomolar inhibition of butyrylcholinesterase ($Ki = 1.09 \pm 0.12$ nM). In addition, compounds **8** and **11** show metal-chelating properties, and reduce the redox activity of chelated Cu^{2+} ions in a Cu-ascorbate redox system. Compounds **8** and **11** decrease intracellular levels of reactive oxygen species, and are not substrates of the active efflux transport system, as determined in Caco2 cells. Compound **11** also protects neuroblastoma SH-SY5Y cells from toxic $A\beta_{1-42}$ species. These data indicate that compounds **8** and **11** are promising multifunctional lead ligands for treatment of Alzheimer's disease.

1. Introduction

Increased life expectancy and ageing of the population has led to higher incidence of age-dependent neurodegenerative disorders. As one of these, Alzheimer's disease (AD) accounts for 60%–70% of cases of senile dementia. The number of patients with AD worldwide is estimated at around 50 million and nearly 10 million new patients are diagnosed every year [1,2]. Dementia associated with AD substantially affects not only the daily life activities of patients, but also their families and society as a whole [3].

Alzheimer's disease is associated with decreased brain levels of the neurotransmitter acetylcholine (ACh). This led to the cholinergic hypothesis of AD, whereby decreased ACh levels are responsible for defects in cholinergic neurotransmission, which affects memory, orientation and judgment, and other cognitive processes [4]. In line with this hypothesis, it was proposed that inhibition of the enzymes involved in ACh breakdown, the cholinesterases (ChEs), would alleviate the symptoms and possibly delay the progression of AD. Accordingly, three out of the four currently approved anti-Alzheimer's drugs are ChE inhibitors: rivastigmine, donepezil and galantamine (Fig. 1A) [5]. These compounds mainly target acetylcholinesterase (AChE), the most abundant ChE in the central nervous system (CNS).

The other ChE in the CNS is butyrylcholinesterase (BChE), which accounts for 20% of the total brain ChE activity under normal conditions. The observation that BChE activity increases during

* Corresponding author.
E-mail address: stanislav.gobec@ffa.uni-lj.si (S. Gobec).
[1] Present address: Institut Laue Langvein, 71 Avenue des Martyrs, 38000 Grenoble, France.

https://doi.org/10.1016/j.ejmech.2018.07.033
0223-5234/

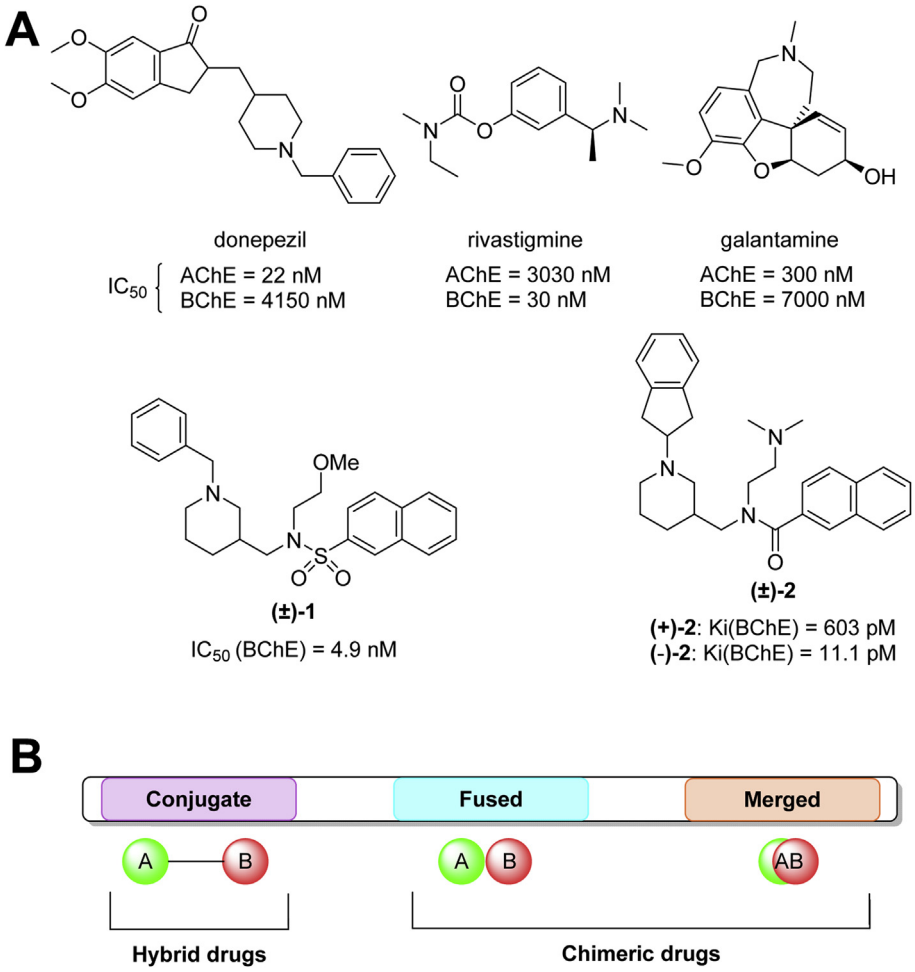

Fig. 1. **(A)** Structures and inhibitory potencies of the approved ChE inhibitors. **(B)** Design of multi-target-directed ligands (adapted from Refs. [27,35]).

progression of AD then led to the hypothesis of BChE as a useful target, at least in the later stages of AD [6–8]. Another advantage of BChE is that unlike AChE, it is not expressed in the peripheral and parasympathic autonomous nervous systems. BChE-specific inhibitors should thus be devoid of the adverse side-effects of AChE-specific inhibitors that limit their dosing in the clinical context [9,10]. Accordingly, selective inhibition of BChE with cymserine analogues elevates ACh levels in the brain, reduces secretion of amyloid β (Aβ) peptide in a human neuronal cell line, and improves cognitive performance in aged rats [11,12]. Several classes of selective BChE inhibitors have been discovered and have been reviewed elsewhere [13]. Recently developed selective reversible BChE inhibitors **1** and **2** (Fig. 1A) improve cognitive functions in models of scopolamine-induced cognitive impairment, without causing acute cholinergic side-effects [14,15]. In line with these data, BChE inhibition can be viewed as an alternative for restoration of cholinergic activity and improvement of cognitive performance for patients with AD [16]. However, inhibition of ChEs is not sufficient for the treatment of patients with AD, as this provides at best an alleviation of symptoms, with no substantial modification of the progression of AD [9].

Fundamental science has provided insights into the complex etiology of AD by showing that in addition to decreases in brain ACh levels, a variety of cellular processes are impaired during the onset and progression of AD. Some of the promising processes to target are oxidative stress [17,18], loss of metal-ion homeostasis [19], and aggregation and accumulation of the Aβ peptide into plaques and oligomers [20,21]. Formation of amyloid plaques affects several molecular processes, as it reduces the amount of functional monomers [22], results in oxidative stress [23], and contributes to loss of metal-ion homeostasis [19]. High concentrations of several important metals (i.e., Cu^{2+}, Zn^{2+}, Fe^{2+}) have indeed been associated with various Aβ structures [23,24]. Alterations to metal biodistributions in pre-synaptic and post-synaptic neurons result in abnormal neurotransmission, altered activities of metal-dependent enzymes, and increased Aβ secretion [19]. Furthermore, complexes of Aβ with redox active ions (i.e., Cu^{2+}, Fe^{2+}) can generate reactive oxygen species (ROS), which can lead to oxidative stress, lipid peroxidation and protein damage. Thus these ions, and especially redox-active Cu^{2+}, represent an interesting target in drug discovery targeted at AD [25]. Intracellular oxidative stress has also been linked to early events in the pathogenesis of AD [26]. Accordingly, drugs with radical scavenging activities hold big promises in the treatment of this devastating disorder.

Treatment strategies for neurodegenerative diseases have long focused on the 'magic bullet' concept. More recently, however, the complex and multilayered pathophysiology of AD has led to the rejection of this paradigm, and instead to a focus on multi-target strategies [27–29]. A variety of multi-target-directed ligands (MTDLs) has since been proposed that target multiple pathways involved in the onset and progression of AD [30,31]. Apart from ChE inhibition, which is the current target for symptomatic relief,

several other activities can be introduced into MTDLs to potentially achieve more effective treatment of AD. The grafting onto ChE inhibitors of pharmacophores that target Aβ aggregation, inhibit monoamine oxidase and BACE1, act on several receptor systems, prevent oxidative stress, and/or chelate metal ions has therefore been explored for the design of disease-modifying MTDLs [32–34].

A variety of strategies has been followed to produce such MTDLs (Fig. 1B). Hybrid drugs can be produced by joining together two pharmacophores through a low-molecular-weight linker. Most recently, MTDLs have been designed where pharmacophores overlap within structurally shared motifs. The degree of overlap can vary from the fusing of one motif directly to another (which results in compounds with high molecular weights) to highly integrated pharmacophores (which produces compounds with lower molecular weights) [35,36].

We reported previously on a series of piperidine-3-ylmethanamine-based selective human (h)BChE inhibitors with low nanomolar and picomolar inhibitory potencies [14,15]. The most potent of these, hBChE inhibitor **2**, has a K_i in the picomolar range, crosses the blood-brain barrier (BBB) *in vivo*, and shows pro-cognitive effects in a scopolamine mouse model of cognitive impairment [15]. In the current study, we describe the design, synthesis and biochemical evaluation of a focused library of BChE inhibitors that include additional antioxidant, metal-chelating and neuroprotective properties. The series of MTDLs presented herein offers a new class of potential ligands for treatment of patients with AD.

2. Results and discussion

2.1. Design

The crystal structures of hBChE with picomolar inhibitor **2** [15] (Fig. 1A) and nitroxoline derivative **3** [37] (Fig. 2A) were used as the starting point for functionalization and further optimisation of multifunctional BChE inhibitors. Briefly, these structures showed three potential positions for introduction of modifications to form highly merged chimeric compounds with overlapping pharmacophores. The first is the cationic sub-site of the active site, contributed to by Trp82 and Glu197, which accommodates the 2-(dimethylamino)ethyl side-chain of compound **2** in the crystal structure (PDB 5NN0). The cation-π interaction between this side-chain and Trp82 is the origin of the exceptional binding affinity of compound **2**. Hence, this part of the molecule was left intact, with a view to the retaining of the BChE inhibitory potency as the principal activity of this series of MTDLs.

The first and the most explored option was the replacement of the naphthalene moiety, which according to the crystal structure with compound **2**, binds in the hydrophobic acyl binding pocket of hBChE (Trp231, Leu286, Val288, Phe398). The crystal structure of hBChE with compound **3** where an 8-hydroxy-5-nitroquinoline moiety replaces the naphthalene moiety of compound **2** illustrates that although it is lipophilic, the acyl binding pocket can accommodate fragments with additional functionalities (e.g., that can provide selective Cu^{2+} chelation, antioxidant activity). We also explored substitution of the 2,3-dihydro-1*H*-indene attached to the piperidine nitrogen that points towards the exit of the active-site gorge, and that does not contribute to any specific interactions with the residues of the active-site gorge. The basicity of the piperidine nitrogen was nevertheless preserved, to maintain the strong cation-π contact with Tyr332, as seen in the crystal structures of hBChE with both compounds **2** and **3**.

The choice of the structural fragments with reported metal chelation, antioxidant or neuroprotective properties was based on their size and the extent of their potential activity in the pathology of AD [38–41]. To limit the molecular weights of the final compounds, and to ensure drug-like properties and the potential to cross the BBB, moieties with low molecular weights were preferred over larger ones. This particularly focused on those for which previous data were available that showed beneficial activity in the context of AD, as well as moieties available either commercially or through rapid synthesis [42]. 8-Hydroxyquinoline (8-HQ) derivatives are widely used in the design of multifunctional ligands due to their potent metal-chelating properties, direct antioxidant activities, and generally neuroprotective and neurorestorative actions [40]. Two derivatives have already been used in clinical trials as anti-AD ligands, where their safety and positive clinical effects on cognition were demonstrated: PBT2 and clioquinol [43,44]. Several derivatives were designed by varying the −COOH substitution position from either 2 or 7, together with the number and the position of the substituents (i.e., OH, NO_2). Known antioxidants were also used to add antioxidant activity, such as Trolox, 4-hydroxycinnamic acid and phenols [23]. Some additional derivatives with phenol groups and nitrogen-free ion pairs that provide metal-ion chelation were also prepared to further probe the chemical space and determine their potential as antioxidants and/or metal chelators.

2.2. Chemistry

Key intermediates for the synthesis of the designed derivatives (amines **4**, **5**, **6b**) were prepared from the readily available nipecotic acid and following procedures reported previously (Table 1, Scheme 1) [45]. Main synthon **5** was coupled with various fragments that have metal-chelating and antioxidant properties, or neuroprotective activity, which provided compounds **8**–**19** and **24**–**28** (Table 1). Some of these fragments are available commercially (e.g., 8-hydroxyquinoline-7-carboxylic acid, 8-hydroxyquinoline-2-carboxylic acid, 4,8-dihydroxyquinoline-2-carboxylic acid) while others (**7a**–**d**) were synthesised in the course of this study, as described in the Supporting Information or in the literature [46]. Coupling of 8-hydroxyquinoline-7-carboxylic acid with **5** using the carbonyldiimidazole (CDI) reagent in anhydrous tetrahydrofuran (THF) resulted in the 8-HQ derivative **8**. For the purpose of comparison with nitroxoline derivative **3** [37], 8-HQ derivative **9** with a methoxyethyl side-chain was also prepared, through the same procedure with CDI. Coupling procedures using *O*-(benzotriazol-1-yl)-*N*,*N*,*N*′,*N*′-tetramethyluronium tetrafluoroborate (TBTU) or 11 [bis(dimethylamino)methylene]-1*H*-1,2,3-triazolo [4,5-*b*]pyridinium 3-oxid hexafluorophosphate (HATU) in the presence of Et_3N as a base were also used to replace the naphthalene ring of the parent inhibitor **2** with 8-HQ derivatives (**10**–**12**), 2-methylimidazo [1,2-*a*]pyridin-8-ol (**17**), and some other fragments (Table 1, compounds **13**–**16**, **18**). Later, the formation of acyl chloride with thionyl chloride was used to activate 2-oxo-2*H*-chromene-3-carboxylic acid, which was reacted with **5** in pyridine as solvent, to yield coumarine analogue **19**. Amine **5** was also combined with acetyl-protected hydroxybenzoic acids and 4-acetoxycinnamic acid using TBTU as the coupling reagent. The acetyl-protected intermediates **20**–**23** that were formed were already partially deacetylated, as shown by proton nuclear magnetic resonance (NMR), and were immediately deprotected in methanolic K_2CO_3 solution, to provide the final phenols **24**–**27**. To determine the influence of the hydroxyl group on the antioxidant and BChE inhibition of novel MTDLs, 4-methoxybezoyl chloride was reacted with **5** to prepare **28**, a methoxy analogue of **26**.

To prepare two derivatives where 2,3-dihydro-1*H*-inden was replaced by other functionalities, **6a** was first debenzylated with cyclohexene in the presence of palladium hydroxide on carbon (Pearlman's catalyst), which yielded crude secondary amine **6b** (see

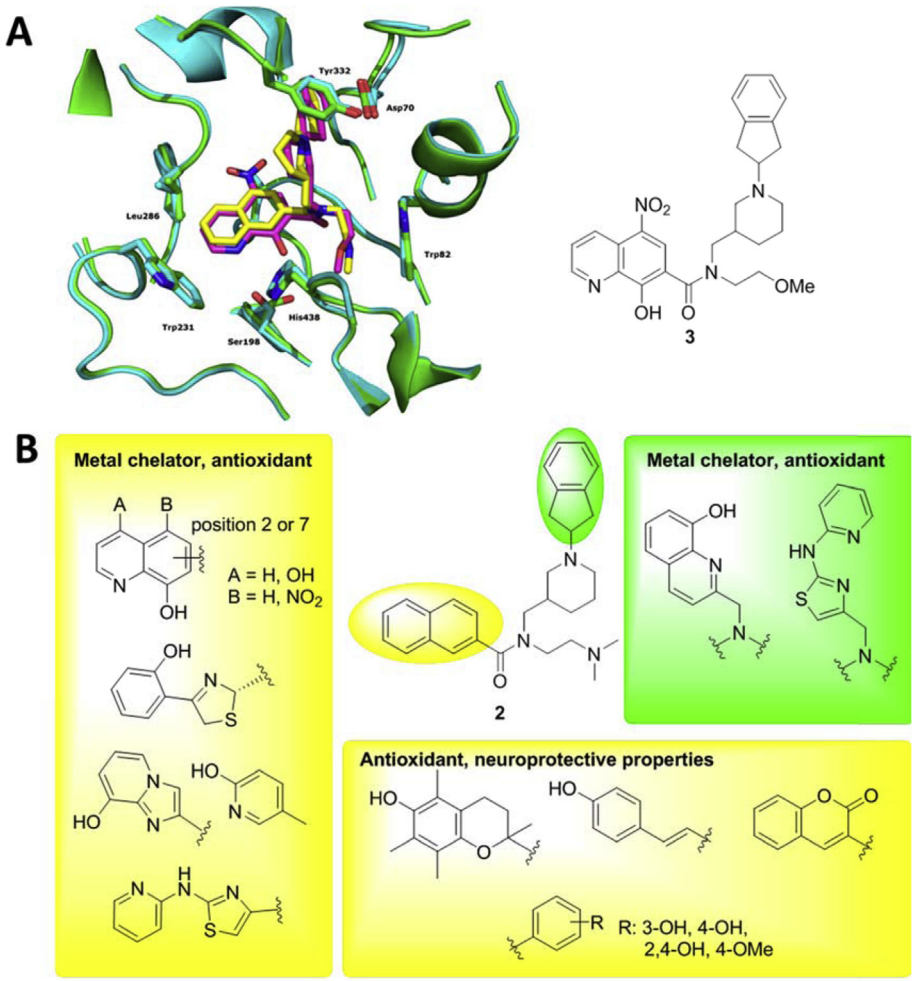

Fig. 2. **(A)** Overlay of the active sites of compounds **2** (yellow) and **3** (magenta) in complex with hBChE (PDB codes 4XII [cyan] and 5NN0 [green]). The structure of compound **3** is also shown. **(B)** Merging the main features of inhibitor **2** with fragments with antioxidant, metal-chelation or neuroprotective properties. (For interpretation of the references to color in this figure legend, the reader is referred to the Web version of this article.)

Supporting Information). Crude **6b** was then alkylated with 4-(chloromethyl)-*N*-(pyridin-2-yl)thiazol-2-amine hydrochloride **7d** (see Supporting Information) in anhydrous dimethylformamide (DMF) using K_2CO_3 as the base, to produce the final amide **29**. Crude **6b** was also reacted with 8-hydroxyquinoline-2-carboxyaldehyde under conditions for reductive amination in the presence of sodium triacetoxyborohydride, to obtain compound **30** at a moderate yield.

2.3. Calculation of physicochemical parameters and ADMET prediction

When designing ligands that are targeted to the CNS with drug-like properties and sufficient penetration through the BBB, it is important to ensure their oral bioavailability and activity at their site of action [42,47]. For each of the synthesised compounds, several physicochemical parameters, molecular descriptors, and absorption, distribution, metabolism, excretion and toxicity (ADMET) properties were calculated using *in-silico* tools and in-house scripts (see Supporting Information, Table S1). All of the derivatives showed calculated LogP <5, and the majority of the structures satisfied the Lipinski rule of five [47], except for a few compounds where the MWs were just above the reference value of 500 Da. Also, for the majority of the derivatives, the calculated polar surface area (PSA) was below the empirical limits for potential BBB penetration (PSA <90 Å) [48], except for nitro derivatives **10** and **12**. Multilayered predictors that take into the account several other parameters to predict BBB penetration and oral bioavailability predicted borderline or moderate CNS penetration and moderate to good absorption in the gastrointestinal tract (e.g., MDCK cell permeability model for BBB; modelled partition coefficient [logBB]; Caco2 cell permeability model for gut-blood barrier; human oral absorption; for details, see Supporting Information, Table S1). All of the compounds had modelled partition coefficients (logBB) above the qualifying lower limit of −1.2 suggested by Ghose et al. [49], and the preferred lower limit (−0.06) was satisfied by 11 of the derivatives. The most problematic were derivatives that did not comply with the general Lipinski rules, or those that were characterised by high PSA. Similar predictions were obtained using the MDCK model, which is considered to be a good approximation for BBB permeability and a useful tool for rapid membrane-permeability screening [50]. In summary, our series of MTDLs were predicted to have adequate ADMET properties, with several of them satisfying different drug-like criteria and having structures that are compatible with brain penetration, as required for their activities in the CNS.

Table 1
Synthesis of derivatives **8**–**19** and **24**–**28**.

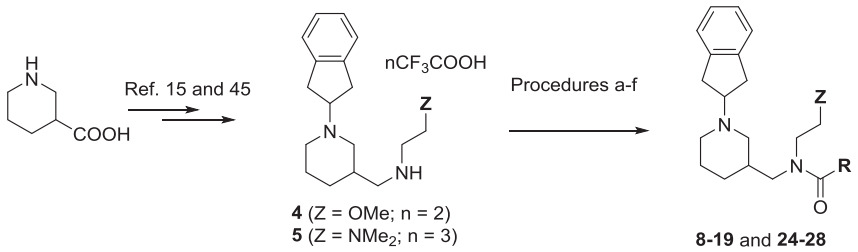

Cpd	Proc.[a]	Z	R	Cpd	Proc.[a]	Z	R
3	Ref. [37]	OMe	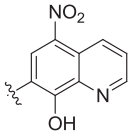	**16**	c	NMe_2	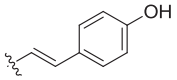
8	a	NMe_2	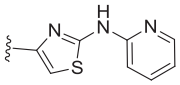	**17**	c	NMe_2	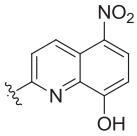
9	a	OMe_2	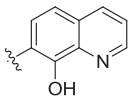	**18**	c	NMe_2	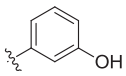
10	b	NMe_2	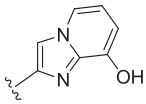	**19**	d	NMe_2	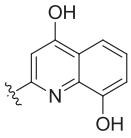
11	c	NMe_2	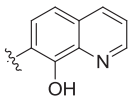	**24**	e	NMe_2	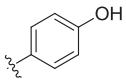
12	c	NMe_2	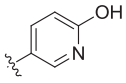	**25**	e	NMe_2	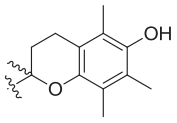
13	c	NMe_2	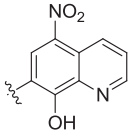	**26**	e	NMe_2	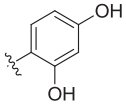
14	c	NMe_2	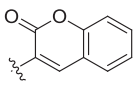	**27**	e	NMe_2	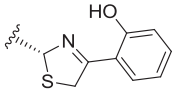
15	c	NMe_2	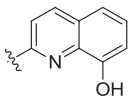	**28**	f	NMe_2	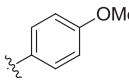

[a] Reagents and conditions: **(a)** (i) 8-hydroxyquinoline-7-carboxylic acid, CDI, anh. THF, 65 °C, 90 min; (ii) **5** (for **8**)/**4** (for **9**), Et_3N, anh. THF, 65 °C, 24 h; **(b)** (i) 8-hydroxy-5-nitroquinoline-7-carboxylic acid, $SOCl_2$, toluene, 80 °C, 24 h; (ii) **5**, Et_3N, CH_2Cl_2, 0 °C, rt, overnight; **(c)** (i) corresponding acid, HATU, Et_3N, MeCN, rt, 30 min; (ii) **5**, Et_3N, MeCN, rt, 24 h; **(d)** (i) 2-oxo-2*H*-chromene-3-carboxylic acid, $SOCl_2$, 80 °C, 4 h; (ii) **5**, Et_3N, CH_2Cl_2, 0 °C, rt, 72 h; **(e)** (i) corresponding acid, TBTU, Et_3N, CH_2Cl_2, 0 °C, 30 min; (ii) **5**, CH_2Cl_2, rt, 24 h, to obtain acetyl protected intermediates **20**–**23**; (iii) K_2CO_3, MeOH, rt, 24 h; **(f)** **5**, Et_3N, 4-methoxybenzoyl chloride, CH_2Cl_2, 0 °C, rt, 16 h.

2.4. Inhibition of cholinesterases

The *in-vitro* hBChE inhibitory potencies of the designed MTDLs were determined using the method of Ellman as done before [15] and the BChE-specific substrate butyrylthiocholine iodide. To address the selectivity of the designed inhibitors towards hBChE, their inhibition of human (h)AChE was also determined under the same assay conditions, but with the AChE-specific substrate

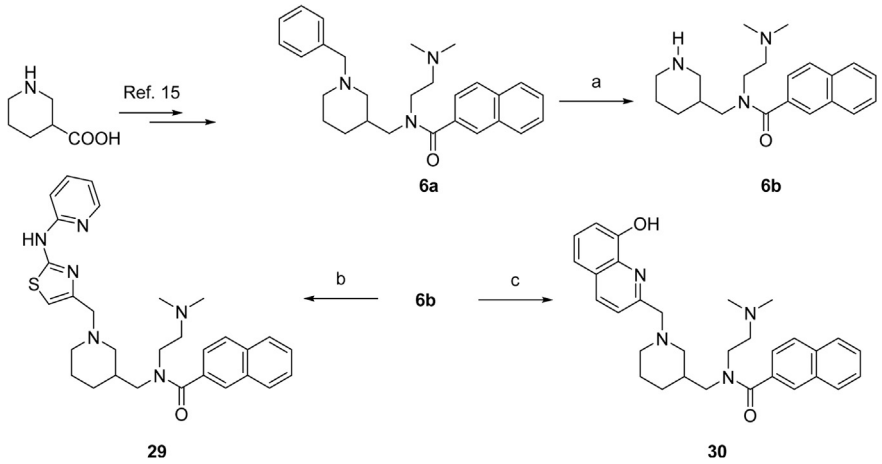

Scheme 1. Reagents and conditions: **(a)** cyclohexene, $Pd(OH)_2/C$, MeOH, 75 °C, 18 h; **(b) 7d**, K_2CO_3, anh. DMF, 50 °C, 16 h; **(c)** 8-hydroxyquinoline-2-carboxyaldehyde, $NaBH(OAc)_3$, AcOH, $ClCH_2CH_2Cl$, rt, 24 h.

acetylthiocholine iodide. All of the derivatives were more or less selective towards hBChE over hAChE (Selectivity ratio, Table 2), with IC_{50} values against hBChE in the micromolar to low nanomolar range (Table 2).

Replacement of the naphthalene ring of compound **2** reduced the BChE inhibitory potency. Such an effect was already noted in our previous studies of sulfonamide and amide analogues, where smaller monocyclic aromatic rings or substituents on the naphthalene were generally associated with lowered inhibitory potencies [14,15]. This effect might be due to steric hindrance and/or the non-optimal fit of the aromatic rings, loss of important T-stacking of naphthalene with Trp231 or alternative binding mode as disused further on [15,51]. However, the IC_{50} values of the best MTDLs reported here were still comparable to those of the *in-vivo* active hBChE inhibitor **1** [14]. On the other hand, the loss of picomolar inhibitory potency was counterbalanced by additional activities that were gained with these modifications. Data from the concise 8-HQ sub-series (**8**–**13**) suggested that the 8-HQ metal-chelating core can be accommodated into the acyl binding pocket. Among these compounds, positional isomers **8** and **11** were equipotent inhibitors, with IC_{50} values of 13.8 ± 0.6 nM and 11.1 ± 0.6 nM, respectively. The introduction of a hydroxyl group at position 4 of 8-hydroxyquinoline-2-carboxamide provided compound **13** (IC_{50}, 28.0 ± 1.3 nM), and did not alter the low nanomolar potency of parent compound **11**. On the other hand, the introduction of a nitro group at position 5 notably reduced the hBChE inhibitory potency (**12**; IC_{50}, 1611.8 ± 123.8 nM). When an additional nitro group was introduced at position 5 of 8-HQ derivative **8**,

Table 2
Cholinesterase inhibitory potencies and radical-scavenging activities (DPPH assay) of the MTDLs.

No	hBChE inhibition IC_{50} ±SEM (nM)[a]	hAChE inhibition %RA[b] at 10 μM	Selectivity ratio[c]	Radical-scavenging DPPH assay EC_{50} (μM)
2 [15]	1.03 ± 0.04 [15]	n.i.[d]	>9709 [15]	n.d.[e]
3 [37]	215 [37]	n.i.[d]	>140 [37]	3448.8 ± 3.7 [37]
8	IC_{50} = 13.8 ± 0.6	n.i.[d]	>725	61.4 ± 7.6
9	265.8 ± 23.2	n.i.[d]	>38	3544.0 ± 262.0
10	28.0 ± 1.3	n.i.[d]	>357	1048.9 ± 76.4
11	IC_{50} = 11.1 ± 0.6	75.8%	>900	544.0 ± 41.5
12	1611.8 ± 123.8	n.i.[d]	>6	1753.3 ± 70.5
13	19.0 ± 1.0	n.i.[d]	>526	74.6 ± 17.3
14	6916.4 ± 203.4	n.i.[d]	>1	264.2 ± 34.5
15	228.6 ± 25.0	72.9%	>44	3233.1 ± 139.4
16	634.5 ± 40.5	n.i.[d]	>15	3475.0 ± 208.6
17	135.0 ± 7.8	n.i.[d]	>74	42.1 ± 1.9
18	20951.3 ± 165.1	n.i.[d]	n.d.[e]	995.0 ± 7.0
19	9.5 ± 0.5	n.i.[d]	>1053	Not active
24	71.0 ± 1.9	n.i.[d]	>141	55.9 ± 4.6
25	2485.1 ± 21.2	n.i.[d]	>4	2862.7 ± 70.3
26	1794.2 ± 45.1	n.i.[d]	>2	2731.0 ± 59.8
27	460.4 ± 29.4	n.i.[d]	>21	389.9 ± 28.7
28	237.0 ± 25.8	n.i.[d]	>42	2625.7 ± 12.0
29	103.1 ± 4.7	n.i.[d]	>96	761.8 ± 15.2
30	48.1 ± 1.4	n.i.[d]	>208	402.4 ± 36.3
Tacrine	23.2 ± 2.9	IC_{50} = 114.8 ± 8.5 nM	5.0	n.d.[e]
Resveratrol	n.d.[e]	n.d.[e]	n.d.[e]	50.1 ± 4.6
Trolox	n.d.[e]	n.d.[e]	n.d.[e]	12.4 ± 0.3

[a] The IC_{50} values are expressed as mean ± standard error of three independent experiments performed in triplicates.
[b] RA, residual activity.
[c] Selectivity ratio: IC_{50} (hAChE)/IC_{50} (hBChE).
[d] ni., no inhibition (RA >80%).
[e] n. d., not determined.

there was no significant change in inhibitory activity (**10**; IC_{50}, 28.0 ± 1.3 nM), as expected from the crystal structure of compound **3** with hBChE [37]. The presence of the 2-(dimethylamino)ethylene side-chain increased the inhibitory potency of **8** to almost 10-fold that of compound **3**, which has a methoxyethyl side-chain. The significance of this modification was also evident from the comparison of the inhibition properties of compound **8** (IC_{50}, 13.8 ± 0.6 nM) and methoxyethyl analogue **9**, where compound **9** had an almost 20-fold higher IC_{50}.

Replacement of the naphthalene ring in compound **14** with Trolox, as the active part of the antioxidant vitamin E, resulted in almost complete loss of ChE inhibitory potency. Introduction of several other potential metal chelators of varying sizes into compounds **15**–**18** notably reduced the hBChE inhibitory potencies (IC_{50}, from 135.0 nM to 20.4 μM). The bulkiness and non-linear conformation of these substituents challenged the fit of the resulting MTDLs into the active-site gorge of hBChE, which would explain their decreased inhibitory potencies. Derivative **19** with the coumarine core was the most potent inhibitor of the series (IC_{50}, 9.5 ± 0.5 nM); however the potency was still in the range of the other 8-HQ derivatives (e.g., **8**, **11**). Compounds **24**–**27** had hydroxybenzene and *p*-hydroxycinnamic moieties that replaced the naphthalene, and these showed nanomolar to low micromolar BChE inhibitory potencies. The most potent hBChE inhibitor in this sub-series with possible antioxidative activity was **24** (IC_{50}, 71.0 ± 1.9 nM), which included *p*-hydroxycinnamic acid. Both 3-hydroxybenzene and 4-hydroxybenzene derivatives (**25**, **26**, respectively) were micromolar inhibitors, whereas the more polar 2,4-dihydroxy derivative **27** inhibited hBChE in the sub-micromolar range. Methoxy derivative **28** was more potent that its hydroxy analogue **26**, which again showed the improved interaction with the binding pocket for substituents with higher lipophilicity.

Replacement of 2,3-dihydro-1*H*-inden with *N*-(pyridin-2-yl)-thiazol-2-amine (**29**; IC_{50}, 103.1 ± 4.7 nM) or 8-HQ (**30**; IC_{50}, 48.1 ± 1.4 nM) also resulted in diminished inhibition of hBChE. The larger entrance to the active-site gorge might accommodate substituents with larger volumes, although the orientation of the two represented fragments was probably similar to the benzyl substituents, which as demonstrated before, did not provide the optimal inhibitory activity seen for 2,3-dihydro-1*H*-inden of inhibitor **2** [15]. However, other beneficial properties were gained that counterbalanced the loss of the BChE inhibitory potency, which defines this series as suitable for further studies. Based on these, the kinetic parameters of hBChE inhibition were determined for compounds **8** and **11** (Table 3).

The selectivity of the compounds towards hBChE in comparison to hAChE can be explained by the differences of their active site composition. The acyl binding pocket of hAChE is lined with two large aminoacid residues (Phe288 and Phe290), which are replaced with smaller Leu286 and Val288 in hBChE. Therefore, hAChE cannot accommodate bigger moieties, such as 8-hydroxyquinoline core of compounds **8** and **11**. This has been demonstrated previously for the hit compound [51], on the basis of which the whole series of selective hBChE inhibitors was designed.

Table 3
Inhibition constants of the most potent hBChE inhibitors **8** and **11**.

No	hBChE inhibition *Ki* (nM)
2 [15]	*Ki* (+)**2** = 603 pM *Ki* (−)**2** = 11.1 pM [15]
8	1.71 ± 0.24 nM[a]
11	1.09 ± 0.12 nM[a]

[a] The *Ki* values were determined for compounds **8** and **11** (Supporting information, Figure S1), which show the most promising multifunctional profile (as discussed below). Both compounds display competitive mode of inhibition. The *Ki* are expressed as mean ± error of three independent experiments.

2.5. Radical-scavenging activity

The increased oxidative stress observed in AD has been addressed in several studies where known antioxidants were introduced into novel multifunctional ligands (e.g., phenols, derivatives of cinnamic acid, resveratrol) [31]. This might have additional symptomatic benefits in AD therapy, and moreover, interference with the progression of AD is also anticipated [18,23]. Several MTDLs reported herein have free phenol groups that can serve as a hydrogen radical ($H^{\bullet}$) or electron donor, and can therefore impart antioxidant potency. The antioxidant activities of the derivatives were determined by measuring free-radical-scavenging using the 2,2-diphenyl-1-picrylhydrazyl (DPPH) radical. DPPH assay is one of the most frequent assays for determination of antioxidant activity due to its low cost, relative speed and simplicity [52]. Antioxidant activity were expressed as an EC_{50} value, which is defined as the effective concentration of an antioxidant required for reduction of 50% of DPPH radical in a solution. The DPPH concentration is selected so, that it is in the linear range of the method (UV–vis spectroscopy). This is the reason why antioxidant values cannot be directly compared with other activities (e.g., enzyme inhibition), but should be interpreted in comparison with known antioxidants assayed in the same manner.

The data from the DPPH assays indicate that all of the derivatives showed antioxidant activity (Table 2). The antioxidant potencies of the best derivatives are comparable to those of resveratrol and Trolox, which were determined under the same assay conditions (EC_{50}, 50.1 ± 4.6 μM; 12.4 ± 0.3 μM; respectively). In the 8-HQ sub-series, derivative **8** (8-hydroxyquinoline7-carboxamide) was the most potent antioxidant, with an EC_{50} of 61.4 ± 7.6 μM. Positional isomer **11** (8-hydroxyquinoline-2-carboxamide) showed an almost 90% reduction in potency, which could stem from changes in the electron densities of the quinolone rings that will depend on the position of the carboxamide substitution. When a nitro group was introduced at the *para* position to the hydroxyl group (i.e., compounds **10** and **12**), the antioxidant potency was reduced, arguably because of the electron-withdrawing effects of this substituent. In contrast, introduction of an additional 4-hydroxy group (-OH) into compound **13** increased the antioxidant activity (EC_{50}, 74.6 ± 17.3 μM). Among the different phenol-containing compounds, analogue **17** included an imidazo [1,2-*a*]pyridin-8-ol moiety, and it was the most potent antioxidant (EC_{50}, 42.1 ± 1.9 μM), followed by derivative **24** (EC_{50}, 55.9 ± 4.6 μM), which contained a fragment of the natural antioxidant 4-hydroxycinnamic acid. Derivative **14** contained the fragment of vitamin E (Trolox), and it showed an 80% reduction in potency in comparison with the standard (Trolox alone). Hydroxybenzene derivatives **25**–**27** showed only moderate to weak antioxidant activities, which were comparable to those of the *N*-(pyridin-2-yl)-thiazol-2-amine derivatives **16** and **29**. This suggested that the electron-withdrawing effect of carboxamide controls the tendency of the phenol groups to donate $H^{\bullet}$. Compounds **16** and **29** showed a 4-fold difference in antioxidant potencies, and contained only the secondary amine with a hydrogen atom that can be a donor of $H^{\bullet}$ or of an electron.

2.6. Co-crystal structure of compound 11 with hBChE

The crystal structure of the complex of 8-HQ derivative **11** with hBChE was solved at 2.6 Å resolution (Supporting Information, Table S2). Co-crystals were obtained by pre-incubation of hBChE

with the racemic mixture of compound **11** at 500 μM (in 1% DMSO) for 3 h, before mixing with the mother liquor and the subsequent equilibration by vapour diffusion, using the hanging-drop geometry. Strong positive electron density was seen in the initial Fo–Fc map for the active sites of the two monomers in the asymmetric unit (Supporting Information, Figure S2A). Both the *R* and *S* enantiomers can occupy the binding site; however, a better fit was obtained with the *R* enantiomer (Fig. 3A). The refined binding pose of compound **11** was similar to that of the previously published parent compound **2** [15], although with notable differences (Fig. 3B). The 8-HQ moiety of **11** was oriented towards the acyl binding pocket, whereas the 2,3-dihydro-1*H*-inden and the piperidine ring spanned from the bottom of the active-site gorge towards the entrance. The positively charged piperidine nitrogen of **11** formed a cation-π interaction with the phenol ring of Tyr332 (distance between the cation and the nearest carbon of the aromatic ring, 4.1 Å for **2**, and 4.2 Å for **11**). The 8-HQ moiety filled the acyl-binding pocket, and interacted with Trp231 *via* perpendicular π-stacking. The hydroxyl group of the 8-HQ moiety was oriented towards the catalytic residues Ser198 and His438, and formed polar contact with Ser198. Importantly, the nitrogen atom of the 2-(dimethylamino)ethylene moiety was located further away from the Trp82 side-chain in comparison to inhibitor **2** (4.2 Å *versus* 3.7 Å). This might explain the lower affinity of compound **11** for hBChE, as compared to compound **2**.

Remarkably, two other inhibitor molecules were bound at the interface between the two monomers in the co-crystal structure (Fig. 4A). This was not observed with the parent compound **2** [15], which was crystallized under the same conditions (using hBChE from the same expression system; i.e., CHO cells), nor with any of the other compounds from the series of piperidine-based selective hBChE inhibitors [14,15,37,51]. Indeed, co-crystals with compound **11** were obtained in a different, and as yet unforeseen, space group for hBChE ($P42_12$). In the native orthorhombic $P2_12_12_1$ crystals, a biological dimer is generated by symmetry operations, wherein the two monomers interact through a four-helix bundle. In the co-crystal with **11**, no biological dimer was found, which indicated that compound **11** can challenge the formation of the four-helix bundle (Fig. 4A). The helices involved in the formation of the four-helix bundle were indeed seen perpendicular to one another in the hBChE/**11** structure, as opposed to parallel to each other in the native structure (Figure S2B–E). Such dramatic changes in the quaternary organisation appear not to result from the crystallisation process, and might have occurred instead during the pre-incubation of hBChE and compound **11**. Disruption of the four-helix bundle yielded no major impact at the ternary level, as attested by the 0.32 Å root-mean-square deviation between the 535 Cα atoms of the apo and holo enzymes. The buried surface area at the new dimerisation interface was smaller than that observed between monomers that formed a biological dimer in orthorhombic crystals (i.e., 2335 *versus* 3296 $Å^2$, respectively). Nonetheless, each of the two compound **11** molecules at the dimerisation interface had ~85% of its molecular surface buried, which contributed to almost 40% of the overall interface. Close-up analysis of the inhibitor pose in the tetragonal crystals (Fig. 4B) revealed that the piperidine ring and the 2,3-dihydro-1*H*-inden moiety were accommodated in a cavity at the surface of the first monomer, while the 8-HQ ring was bound in another cavity of the second monomer. At the surface of the first monomer, the piperidine ring was lain over the backbone and side-chain atoms of Asp375 and Trp376, respectively, and the 2,3-dihydro-1*H*-inden was accommodated in a hydrophobic groove that was lined by residues His372, Tyr373, Val377, Gln517, Gln518 and Phe521. The positively charged dimethylamino moiety of compound **11** was positioned above the quinoline nitrogen (distance between nitrogens, 2.8 Å). At the surface of the second monomer, the 8-HQ ring of compound **11** was fit into a shallow groove that was contributed to by the side-chains of Ile462, Leu463, Arg470 and Glu482, and the Leu503–Thr508 loop. No H-bond was observed between compound **11** and hBChE, which indicated that the contribution of compound **11** to the formation of the tetragonal crystals of hBChE was purely entropic. The overall conformation of the interface ligand differed greatly from the active-site conformation, as was evident from the superposition of the binding poses (Fig. 4C).

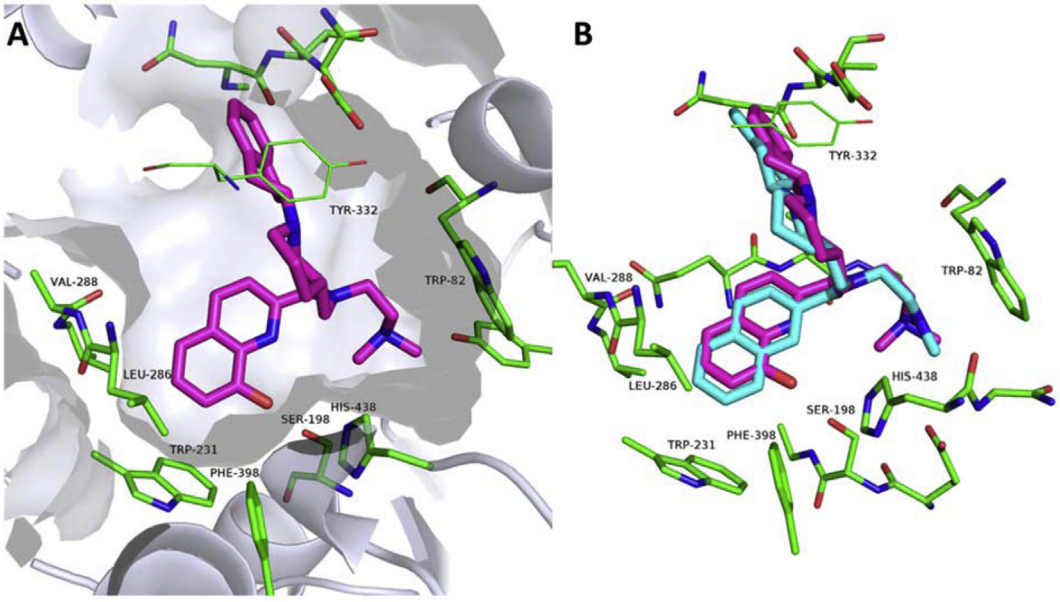

Fig. 3. Crystal structure of compound **11** bound in the active site of hBChE (PDB code 6F7Q). **(A)** Binding mode of selective hBChE inhibitor **11**. Compound **11** is shown as magenta sticks; important active site residues are shown as green sticks. **(B)** Alignment of the crystal structures of compound **11** (magenta) and the parent compound **2** (cyan) in the active site of hBChE. (For interpretation of the references to color in this figure legend, the reader is referred to the Web version of this article.)

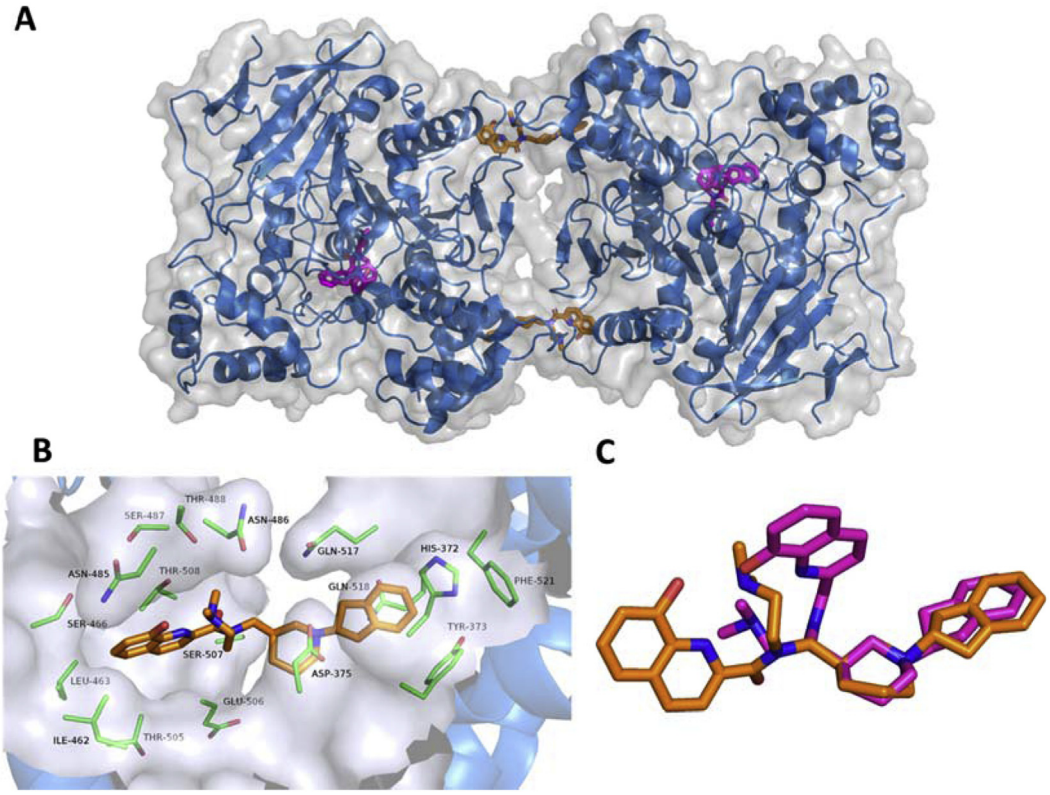

Fig. 4. Binding of 8-HQ derivative **11** to the interface of the two hBChE monomers. The 8-HQ are shown as sticks. Compound **11** located in the active-site is magenta, while the one at the interfaces of the monomers is orange. The amino acids are shown as green sticks. **(A)** Overall view of the crystal structure of compound **11** in complex with the hBChE dimer. The protein monomers are shown as blue ribbon models with a grey surface. **(B)** Close-up view of the interface binding site of compound **11** at the interface between two hBChE monomers. **(C)** Superposition of compound **11** from the active site of hBChE (magenta) and from the interface (orange). (For interpretation of the references to color in this figure legend, the reader is referred to the Web version of this article.)

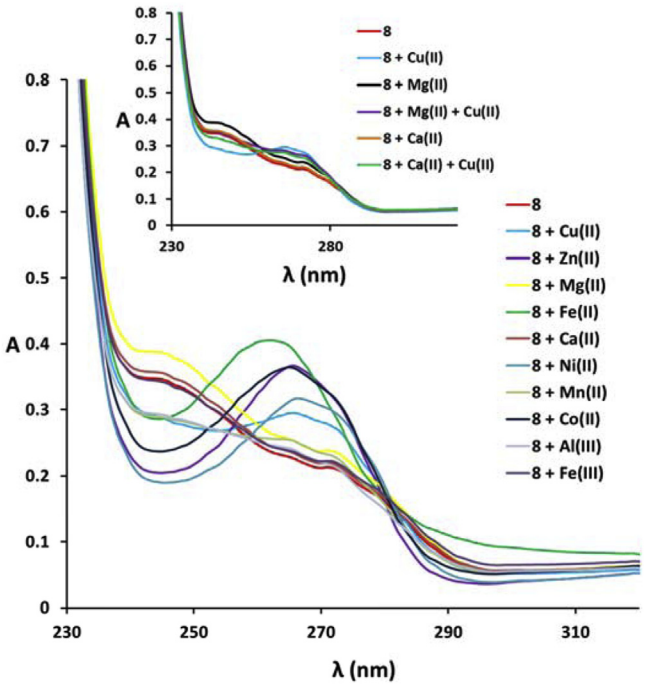

Fig. 5. Metal-chelation properties of compound **8**. Absorption spectra changes for **8** incubated with different metal ions at equimolar concentrations. Inset: Changes in the spectra for Mg^{2+}/Ca^{2+}-**8** complexes after the addition of Cu^{2+} at equimolar concentrations. Only the spectra of the biologically relevant Ca^{2+} and Mg^{2+} are given.

2.7. Chelating properties of compounds 8, 11 and 17

Given their activities on the selected targets (i.e., hBChE inhibition and radical scavenging) and their predicted favourable ADMET properties, the three compounds **8**, **11** and **17** were selected for further studies. The complexing of metal ions by these compounds was investigated using UV–vis spectroscopy measurements at 30 μM compound concentration [37]. This concentration was selected to obtain spectra in the linear range of the method (i.e., UV–Vis spectroscopy). The addition of equimolar amounts of metal ions (i.e., $CuCl_2$, $CaCl_2$, $MgCl_2$, $ZnCl_2$, $CoCl_2$, $NiCl_2$, $MnCl_2$, $FeCl_2$, $FeCl_3$, $AlCl_3$) to solutions of these test compounds resulted in changes in the absorbance spectra between 230 nm and 320 nm if the ligand-metal complex was formed, in comparison to the blank untreated sample. Compound **8** chelated several of these metal ions, including the biologically less relevant Co^{2+}, Ni^{2+} and Al^{3+}, and the more important Cu^{2+}, Zn^{2+} and Fe^{2+}, which are found in Aβ aggregates and can contribute to toxicity and oxidative stress through generation of ROS. The absorbance spectra were not changed upon addition of Ca^{2+} and Fe^{3+}, and only minor changes were seen upon addition of Mg^{2+} (Fig. 5). Similar observations were made for **11**, although the alterations to the absorbance spectra were less obvious and did not allow conclusions about the chelation of ions by compound **11** (Supporting Information, Figure S3). Nonetheless, chelation of Cu^{2+} and Ni^{2+} was evident from the shift in the absorbance maximum at 255 nm and the shoulder that appeared around 270 nm upon mixing with the compound **11**. Selective hBChE inhibitor **17** was devoid of any chelating capacity under the conditions used here, and was therefore not used in the subsequent characterisations.

Cu^{2+} is one of the central ions involved in Aβ aggregation and redox cycling, and accordingly, it has been targeted by many experimental drugs [53–55]. The selectivity of chelators towards Cu^{2+} over other metals was determined, to ensure that the homeostasis of these would not be perturbed, as this might modify cellular metabolism and other functions, especially if the concentrations of the biologically important Ca^{2+} and Mg^{2+} were affected. Equimolar amounts of $CuCl_2$ were added to solutions of **8** and **11** (30 μM, 1% DMSO) that had previously been incubated with the investigated metal ions. The absorbance spectra of the complexes of compound **8** with other metals shifted towards the spectra of Cu^{2+}-**8** for Ca^{2+}, Mg^{2+}, Al^{3+} and Mn^{2+} ions (Fig. 5, inset). The non-selective chelation patterns of compound **8** observed might also be beneficial here, as targeting the other metal ions that are involved in the pathological changes of AD is also desired (e.g., Zn^{2+}, Fe^{2+}) [56].

Unambiguous determination of Cu^{2+} selectivity for compound **11** was not possible due to the small changes in the absorbance spectra before and after addition of $CuCl_2$. These data might be explained by low stability of the complexes formed, small changes in electronic densities and related absorbance properties, and equilibria between several species.

To determine the binding stoichiometry, these compounds were incubated with increasing concentrations of Cu^{2+} (Supporting Information, Figures S4, S5). Incremental additions of $CuCl_2$ to 30 μM buffered solution of compound **8** resulted in increases in the absorbance at 266 nm. The absorbance changes at 226 nm were plotted relative to the Cu^{2+}-**8** M ratios, and the distal parts of the curve (as approximations to tangents) gave an intercept of approximately 1.3, which suggested that one molecule of compound **8** binds one Cu^{2+} (Figure S4). 8-HQ derivatives would typically result in a ratio of 0.5, which represent the binding of one divalent ion to two molecules of 8-HQ, as observed before with clioquinol [57]. However, several reports have also show presence of 1:1 complexes for 8-HQ analogues (e.g., PBT2) [58]. Increasing concentrations of Cu^{2+} also resulted in changes in the absorbance spectra of compound **11**. However, the binding stoichiometry could not be determined here, as the changes in the spectra did not increase linearly with increasing Cu^{2+} concentrations (Figure S5). These deviations from the typical binding stoichiometry might be explained by the presence of the 2-(dimethylamino)ethyl side-chain, which can interact directly with metal ions located near the 8-HQ core or with the quinoline nitrogen.

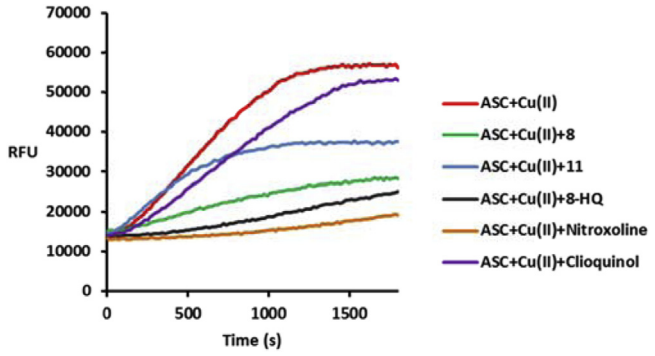

Fig. 6. Ascorbate assay, showing the fluorescence intensity of 7-hydroxy-CCA after incubation of CCA ascorbate with Cu^{2+} (red), compound **8** (green), compound **11** (blue), 8-hydroxyquinoline (black), nitroxoline (orange) and clioquinol (magenta). The ligand (40 μM in the form of salt with HCl) to Cu^{2+} ratio was 2:1. Each experiment was completed in triplicate and the average values are represented as lines. (For interpretation of the references to color in this figure legend, the reader is referred to the Web version of this article.)

Production of ROS by redox-active ions (e.g., Cu(II) ions) in complex with Aβ in brain significantly contributes to the increased oxidative stress in the AD brain. To determine whether compounds **8** and **11** bind Cu(II) and limit hydroxyl radical production in presence of oxygen, the Cu-ascorbate redox system was used as a complimentary antioxidant assay. This system mimics the high levels of oxygen and ascorbate present in the brain [59], and measures the production of hydroxyl radicals through hydroxylation of coumarin-3-carboxylic acid (CCA) to form fluorescent 7-hydroxy-CCA. In the absence of any chelators, a free hydroxyl radical is produced, with the 7-hydroxy-CCA fluorescence reaching a plateau after 20 min (Fig. 6, red line). The production of hydroxyl radical was lowered when compounds **8** and **11** were co-incubated with the Cu-ascorbate system, which indicated that these MTDLs can inhibit the production of hydroxyl radical via metal complexation, along with compounds' antioxidant activity. Compounds **8** and **11** are more potent antioxidants in comparison to clioquinol, yet less effective than 8-hydroxyquinoline itself [60,61].

2.8. Cytotoxicity and neuroprotective activity against ROS and $A\beta_{1-42}$

To gain further insight into the therapeutic potential of these selected compounds, their cell viability and neuroprotective activities against $A\beta_{1-42}$-induced toxicity and oxidative stress were determined using the SH-SY5Y neuroblastoma cell line. The colorimetric 3-(4,5-dimethylthiazol-2-yl)-5-(3-carboxymethoxyphenyl)-2-(4-sulfophenyl)-2*H*-tetrazolium (MTS) assay was performed to examine the potential cytotoxic effects of these compounds. Compounds **8** and **11** showed concentration-dependent cytotoxicities, with LD_{50} values of 9.55 μM and 9.70 μM (Fig. 7), respectively (means of at least three independent experiments), which is in the same range as that of *in vivo* active parent compound **2** [15]. The cytotoxicity in the low micromolar range might seem problematic in terms of safety. However, the LD_{50} values are >700-fold greater than the concentrations needed to achieve 50% *in-vitro* inhibition of hBChE. The antioxidant activity cannot be directly compared with the cytotoxicity assay. The assays differ in the media used (methanol solution for the former and aqueous cell media for the latter), thus the cytotoxicity values lower than the EC_{50} values in DPPH assay do not directly mean the compounds are cytotoxic at concentrations effective in the antioxidant assay. In comparison to known natural antioxidants assayed herein (resveratrol and Trolox), compounds **8** and **11** are equipotent in the DPPH assay. Neuroprotective effects of α-tocopherol against oxidative stress have been described at nanomolar concentrations [62], with typical concentrations of antioxidants, (e.g., tocopherols) in human brain in low nanomol/kg of tissue [63]. Given the low effective concentrations of antioxidants, the cytotoxicity in the micromolar range does not represent any major impairment.

The $A\beta_{1-42}$ isoform is the most amyloidogenic and most abundant form of the Aβ peptide in senile plaques, and this was used as the model peptide for the induction of cytotoxicity [20]. Treatment of SH-SY5Y cells for 48 h with 5 μM pre-aggregated $A\beta_{1-42}$ resulted in reduced cell viability, compared to the control. As can be seen in Fig. 8A, compound **11** had a neuroprotective effect at 1 μM, whereas compound **8** showed only a weaker trend.

The intracellular antioxidant activity was then studied using the cell permeable non-fluorescent 2,7-dichlorodihydrofluorescein diacetate probe, which passively diffuses into cells and is deacetylated to form the non-fluorescent 2,7-dichlorodihydrofluorescein. In the presence of ROS, 2,7-dichlorodihydrofluorescein is oxidised to the highly fluorescent 2′,7′-dichlorodihydrofluorescein, which is trapped inside the cells [64]. After acute exposure to H_2O_2, the levels

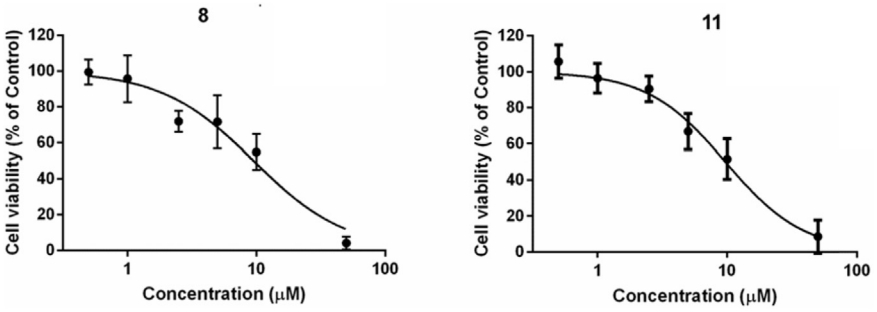

Fig. 7. Cytotoxicity profiles of compounds **8** and **11**. SH-SY5Y cells were incubated with increasing concentrations of the 8-HQ derivatives **8** and **11** (0.5–50 μM). After 48 h, cell viability was evaluated using the MTS assay. The control group (DMSO) was considered as 100% cell viability. The assays were carried out in quadruplicate. The data are means ± SD of at least three independent experiments.

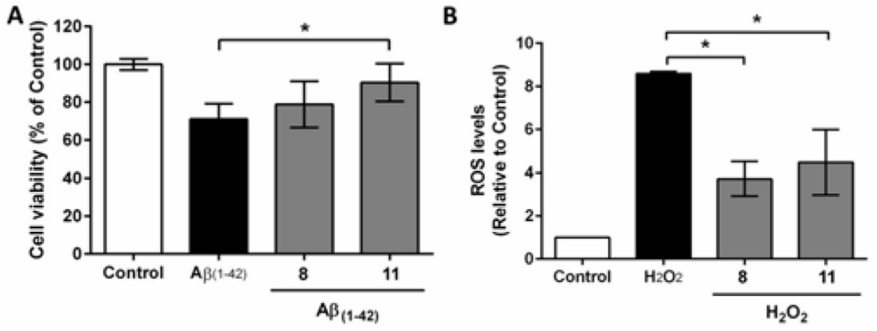

Fig. 8. Neuroprotective activities of compounds **8** and **11** against $A\beta_{1-42}$-induced toxicity **(A)**, and effects on intracellular ROS levels **(B)**. **(A)** Cells were treated with $A\beta_{1-42}$ (5 μM) in the absence and presence of compounds **8** and **11** (1 μM). The control group (DMSO) was considered as 100% cell viability. The assays were carried out in quadruplicate. The data are means ± SD of three independent experiments. $^{*}p < 0.05$. **(B)** SH-SY5Y cells were pretreated in the absence (control) and presence of compounds **8** and **11** (5 μM) for 30 min, followed by treatment with H_2O_2 (500 μM) for an additional 90 min. The ROS levels were measured by 2′,7′-dichlorodihydrofluorescein fluorescence intensity and normalised to the control cells. The assays were carried out in quadruplicate. The data are means ± SD of three independent experiments. $^{*}p < 0.05$.

intracellular ROS were highly increased (Fig. 8B). Compounds **8** and **11** reduced the levels of ROS, thus indicating that they are both effective antioxidants at the cellular level.

2.9. Permeability studies in Caco2 cells and the PAMPA-BBB system

To reach their site of action, and thus show activity in the CNS, drugs must permeate the BBB, i.e., the barrier between the blood and the brain tissue that regulates neuronal homeostasis and limits the access of compounds from the outer environment into the brain tissue [42]. The potential of 8-HQ derivatives **8** and **11** to cross the BBB was also estimated in parallel artificial membrane permeation assay (PAMPA). High permeability expressed as effective permeability (log*Pe*), was predicted for compounds **8** and **11** in this high-throughput assay [65]. The log*Pe* values for compounds **8** and **11** were −4.93 and −4.97, respectively, in comparison to the reference drugs used (log*Pe* (theophylline), −6.71, low BBB permeability; log*Pe* (propranolol), −4.66, high BBB permeability).

Several membrane proteins, like P-glycoprotein and breast-cancer-resistance protein, also limit exposure of the brain *via* active extrusion of exogenous substances from the CNS. To determine the effects of active transport on the permeability of compounds **8** and **11**, simple bidirectional permeability measurements were performed using Caco2 cells that expressed these two proteins [42]. The permeabilities (P_{app}) were determined in both the eliminatory (A–B) and absorptive (B–A) directions, and the efflux ratios ($P_{app(B-A)}/P_{app(A-B)}$) were calculated (Table 4). The $P_{app(B-A)}$ and $P_{app(A-B)}$ permeability values for compounds **8** and **11** were in the same range. Their efflux ratios of <2 suggested that compounds **8** and **11** permeate mainly by passive diffusion or paracellular permeation, and that no active efflux transport should impede their distribution into the CNS [66]. Additionally, the permeability coefficients measured in the absorptive direction were comparable to those of highly permeable drugs like ketoprofen, naproxen and propranolol, which were measured in the same laboratory under the same conditions [67]. As reported by Summerfield et al., molecules with low efflux ratios and high permeabilities tend to also show good CNS penetration [68].

Table 4
Caco2 permeabilities of compounds **8** and **11**.

Compound	$P_{app(B-A)}$[a]	$P_{app(A-B)}$[b]	Efflux ratio ($P_{app(B-A)}/P_{app(A-B)}$)
8	22.8 ± 0.9	15.1 ± 0.6	1.5
11	35.1 ± 0.9	21.5 ± 0.8	1.6

[a] Permeability in the absorptive direction ($\times 10^{-6}$ cm s^{-1}).
[b] Permeability in the eliminatory direction ($\times 10^{-6}$ cm s^{-1}). The data are means ± SD from four replicates.

3. Conclusions

In conclusion, a series of highly merged chimeric MTDLs was designed based on selective hBChE inhibitor **2**. Biological evaluation of these MTDLs showed balanced hBChE inhibition and radical scavenging for several of them. The crystal structure of compound **11** in complex with hBChE revealed the molecular basis for its low nanomolar inhibition, and demonstrated that polar fragments with additional anti-AD activities can be positioned in the acyl-binding pocket of hBChE. The 8-HQ derivatives **8** and **11** showed promising ion-chelating properties, and lowered redox cycling of

chelated Cu^{2+} ions. Additionally, compounds **8** and **11** decreased intracellular levels of ROS after acute treatment with H_2O_2, and protected cells to some extent from toxic $A\beta_{1-42}$ species. Compounds **8** and **11** also showed potential to cross the BBB, and were not substrates for any efflux transport system that might limit their penetration into the brain, as determined in Caco2 cells. This multifunctional profile suggests that compounds **8** and **11** are promising ligands for further development of MTDL drug candidates for the treatment of patients with AD.

4. Experimental methods

4.1. General chemistry methods

The solvents and reagents used for these syntheses were purchased from commercial sources (i.e., Acros Organics, Sigma Aldrich, TCI Europe, Merck, Carlo Erba, Apollo Scientific) and were used as provided, unless indicated otherwise. Analytical thin-layer chromatography was performed on Merck Silica Gel aluminium sheets (60 F254, 0.20 mm), with visualisation using UV light (254 nm) and/or visualisation reagents. Flash column chromatography was performed on Merck Silica Gel 60 (particle size 0.040–0.063 mm, 230–400 mesh). ^{1}H NMR and ^{13}C spectra were recorded at 400 MHz and 100 MHz, respectively, on a Bruker Avance III NMR spectrometer (Bruker Corporation, Billerica, MA, USA) at 295 K, unless indicated otherwise. The chemical shifts (δ) are reported in parts per million (ppm) and are referenced to the deuterated solvent used. Due to the various conformations (rotamers) in solution at room temperature, the number of signals in the ^{13}C spectra exceeded the number of carbon atoms for the majority of these compounds. Also, the ^{1}H spectra exhibit the same phenomena where partial H signals integrations are observed. This was also observed in the literature and in our previous studies [69,70]. ^{13}C NMR spectra could not be obtained for all of the compounds due to the poor relaxation of the carbon atoms, even at elevated temperature (353 K) and in various solvents (e.g., DMSO-d_6, TFA-*d*, $CDCl_3$). Mass spectrometry (MS) measurements were performed on an Advion Expression CMS mass spectrometer (Advion, Ithaca, NY, USA). High-resolution mass measurements (HRMS) were performed on a VG Analytical Autospec Q Micromass mass spectrometer (Fisons, VG Analytical, Manchester, UK) at the Jožef Stefan Insitute, Ljubljana, Slovenia. Analytical reversed-phase HPLC analyses were performed on a Thermo Scientific Dionex UltiMate 3000 modular system (Thermo Fisher Scientific Inc., Waltham, MA, USA). The general HPLC method used a Thermo Scientific Accucore C18 column (4.6 × 100 mm, 2.6 μm) thermostated at 25 °C, with: injection volume, 15 μL; sample, 0.2 mg/mL in MeCN; flow rate, 1.0 mL/min; detector λ, 254 nm; mobile phase A, 0.1% TFA (v/v) in water; mobile phase B, MeCN. Gradient (for mobile phase B): 0–10 min, 10%–90%; 10–14 min, 90%; 14–15 min, 90%–10%. The purities of the tested compounds were established to be ≥ 95%, as determined by HPLC. The tested compounds were examined for known classes of assay interference compounds and were not classified as Pan Assay Interference Compounds (Supporting Information, Table S1).

4.2. General procedure A: HATU coupling

The appropriate acid (1.0 eq.), HATU (1.2 eq.) and Et_3N (1.1 eq.) were stirred in MeCN (20 mL) at room temperature for 30 min. To the resulting mixture, a solution of **5** (1.0 eq.) and Et_3N (5.0 eq.) in MeCN (10 mL) was added, and the mixture was stirred at room temperature for 24 h. The solvent was evaporated, and the residue was dissolved in CH_2Cl_2 (80 mL) and transferred into a separating funnel. The organic phase was washed with saturated aqueous $NaHCO_3$ solution (50 mL), water (3 × 50 mL), and saturated brine solution (50 mL), dried over anhydrous Na_2SO_4, filtered, and evaporated under reduced pressure. The residue was purified by flash column chromatograph and/or reversed-phase column chromatography (Isolera Biotage system, SNAP Biotage KP-18-HS column) using a gradient of 0.1% TFA (aq. sol) and MeCN as eluent. After the reversed-phase column chromatography, the fractions containing the product were combined and the organic solvent was evaporated under reduced pressure. The remaining aqueous solution was made alkaline using saturated aqueous $NaHCO_3$ solution (30 mL), transferred into a separating funnel, and extracted with CH_2Cl_2 (50 mL). The organic phase was dried over anhydrous Na_2SO_4, filtered, and evaporated under reduced pressure.

4.3. General procedure B: TBTU coupling

To the solution of the suitable acetylated acid (e.g., 3-acetoxybenzoic acid, 4-acetoxybenzoic acid, 2,4-diacetoxybenzoic acid) or 4-acetoxycinnamic acid (1.0 eq.) in CH_2Cl_2 (30 mL) at 0 °C, TBTU (1.1 eq.) and Et_3N (5.0 eq.) were added, and stirred at 0 °C for 30 min. To the resulting mixture **5** (1.1 eq.) was added, and the mixture was stirred at room temperature for 24 h. The reaction mixture was then transferred into a separating funnel. The organic phase was washed with saturated aqueous $NaHCO_3$ solution (30 mL) and saturated brine solution (30 mL), dried over anhydrous Na_2SO_4, filtered, and evaporated under reduced pressure. The residue was purified by column chromatography using CH_2Cl_2/MeOH (v/v, 9/1) as eluent. The fractions containing the product were combined to obtain the compounds, which were immediately used in the next step.

4.4. General procedure C: removal of acetyl group

To a solution of acetate **20**–**23** (1.0 eq.) in MeOH (20 mL), K_2CO_3 (5.0 eq.) was added and the mixture was stirred at room temperature for 24 h. The solvent was evaporated, and the residue was dissolved in water (30 mL), acidified with 1 M HCl to pH 7, and extracted with CH_2Cl_2 (3 × 40 mL). The combined organic layers were dried over anhydrous Na_2SO_4, filtered, and evaporated under reduced pressure, to obtain the pure compounds, unless indicated otherwise.

The detailed experimental procedures on the synthesis of amine **6b** and its precursors are provided in the Supporting Information.

4.5. Syntheses of MTDLs

4.5.1. (±)-N-((1-(2,3-dihydro-1H-inden-2-yl)piperidin-3-yl)methyl)-N-(2-(dimethylamino)ethyl)-8-hydroxyquinoline-7-carboxamide (**8**)

A solution of 8-hydroxyquinoline-7-carboxylic acid (230 mg, 1.22 mmol, 1.33 eq.) and CDI (197 mg, 1.22 mmol, 1.33 eq.) in anhydrous THF (15 mL) was stirred under an argon atmosphere at 65 °C for 90 min. To the resulting mixture, a solution of **5** [15] (589 mg, 0.92 mmol, 1.0 eq.) and Et_3N (634 μL, 4.58 mmol, 5.0 eq.) in anhydrous THF (10 mL) was added, and the mixture was stirred at 65 °C for 24 h. The solvent was evaporated, and the residue was dissolved in CH_2Cl_2 (50 mL) and transferred into a separating funnel. The organic phase was washed with saturated aqueous $NaHCO_3$ solution (3 × 50 mL), water (2 × 50 mL) and saturated brine solution (50 mL), dried over anhydrous Na_2SO_4, filtered, and evaporated under reduced pressure. The solvent was evaporated and the residue was purified by reversed-phase column chromatography (Isolera Biotage system, SNAP Biotage KP-18-HS column) using a gradient of 0.1% TFA (aq. sol) and MeCN as eluent. Fractions containing the product were combined and the organic solvent was

evaporated under reduced pressure. The remaining aqueous solution was made alkaline using saturated aqueous $NaHCO_3$ solution (30 mL), transferred into a separating funnel, and extracted with CH_2Cl_2 (50 mL). The organic phase was dried over anhydrous Na_2SO_4, filtered, and evaporated under reduced pressure. The residue was purified by reversed-phase column chromatography as described for compound **9**.

Yield: 7% (23 mg); off-white solid, mp 76–79 °C; Rf = 0.19 (CH_2Cl_2/MeOH = 9/1 + 0.3% NH_3 (25% aq. sol), v/v); ^{1}H NMR (400 MHz, acetone-d_6): δ 0.69 (bs, 0.4H), 1.15 (bs, 0.6H), 1.38–1.75 (m, 3H), 1.81–2.02 (m, 6H), 2.27–2.44 (m, 3H), 2.61–3.78 (m, 14H), 7.10–7.20 (m, 4H), 7.36–7.48 (m, 2H), 7.60 (dd, *J* = 8.3, 4.2 Hz, 1H), 8.34 (dd, *J* = 8.3, 1.4 Hz, 1H), 8.88 (dd, *J* = 4.0, 1.2 Hz, 1H); ^{13}C NMR (100 MHz, DMSO-d_6): δ 24.25, 24.52, 28.17, 34.28, 34.69, 36.06, 36.38, 36.54, 44.93, 45.39, 45.79, 47.60, 51.34, 51.68, 52.06, 55.04, 55.43, 56.15, 57.38, 66.23, 66.82, 117.67, 117.77, 120.30, 120.71, 122.35, 124.07, 124.17, 124.30, 126.10, 126.35, 126.51, 128.43, 128.51, 136.17, 138.14, 141.46, 141.54, 141.66, 148.39, 148.63, 148.72, 168.35, 168.50; ESI-HRMS *m/z* calcd. for $C_{29}H_{37}N_4O_2$ $[M+H]^+$ 473.2917, found 473.2927; IR (ATR) υ = 2939, 2792, 1614, 1503, 1460, 1378, 1252, 1162, 1141, 1115, 1066, 1015, 940, 828, 752 cm^{-1}; HPLC purity, 97.0% at 254 nm (t_R = 4.54 min).

4.5.2. (±)-N-((1-(2,3-dihydro-1H-inden-2-yl)piperidin-3-yl)methyl)-8-hydroxy-N-(2-methoxyethyl)quinoline-7-carboxamide (**9**)

A solution of 8-hydroxyquinoline-7-carboxylic acid (80 mg, 0.42 mmol, 1.0 eq) and CDI (69 mg, 0.42 mmol, 1.0 eq.) in anhydrous THF (15 mL) was stirred under an argon atmosphere at 65 °C for 90 min. To the resulting mixture, a solution of **4** (186 mg, 0.36 mmol, 0.85 eq.) and Et_3N (176 μL, 1.27 mmol, 3.0 eq.) in anhydrous THF (5 mL) was added, and the mixture was stirred at 65 °C for 24 h. The solvent was evaporated, and the residue was purified by reversed-phase column chromatography, as described for compound **8**.

Yield: 19% (32 mg); pale yellow solid, mp 61–63 °C; Rf = 0.34 (CH_2Cl_2/MeOH = 9/1 + 0.3% NH_3 (25% aq. sol), v/v); ^{1}H NMR (400 MHz, $CDCl_3$): δ 0.62 (bs, 0.4H), 1.15 (bs, 0.6H), 1.51–2.20 (m, 6H), 2.80–3.80 (m, 17H), 7.10–7.16 (m, 4H), 7.34 (d, *J* = 8.3 Hz, 1H), 7.43 (bs, 1H), 7.45 (dd, *J* = 8.3, 4.1 Hz, 1H), 8.13 (dd, *J* = 8.3, 1.6 Hz, 1H), 8.80 (dd, *J* = 4.3, 1.6 Hz, 1H); ^{13}C NMR (100 MHz, $CDCl_3$): δ 24.98, 28.55, 35.04, 36.97, 37.07, 45.12, 47.86, 48.36, 52.19, 56.01, 58.90, 67.33, 70.71, 118.28, 119.01, 122.54, 124.37, 124.42, 126.38, 126.98, 128.65, 136.20, 138.10, 141.57, 141.60, 148.61, 169.27; ESI-HRMS *m/z* calcd. for $C_{28}H_{34}N_3O_3$ $[M+H]^+$ 460.2600, found 460.2589; IR (ATR) υ = 2929, 1601, 1584, 1543, 1502, 1442, 1382, 1301, 1252, 1195, 1108, 1020, 827, 735, 681 cm^{-1}; HPLC purity, 98.4% at 254 nm (t_R = 5.42 min).

4.5.3. (±)-N-((1-(2,3-dihydro-1H-inden-2-yl)piperidin-3-yl)methyl)-N-(2-(dimethylamino)ethyl)-8-hydroxy-5-nitroquinoline-7-carboxamide (**10**)

This compound was prepared following a procedure described before for a series of nitroxoline derivatives [37]. In a 100-mL round-bottomed flask, amine **5** [15] (220 mg, 0.34 mmol, 0.8 equiv.) was dissolved in CH_2Cl_2 (50 mL), and cooled to 0 °C Et_3N (297 μL, 2.14 mmol, 4.0 equiv.) and previously prepared 8-hydroxy-5-nitroquinoline-7-carbonyl chloride [37] (starting from 8-hydroxy-5-nitroquinoline-7-carboxylic acid: 100 mg, 0.43 mmol, 1.0 equiv.) were added at 0 °C. The resulting yellow solution was stirred for 24 h at room temperature. The mixture was then transferred into a separating funnel and washed with a saturated aqueous $NaHCO_3$ solution (2 × 30 mL) and saturated brine solution (30 mL), dried over anhydrous Na_2SO_4, filtered, and evaporated under reduced pressure. The residue was purified by column chromatography using CH_2Cl_2/MeOH (v/v, 9/1) + 0.3% NH_3 (25% aq. sol) as eluent, and subsequently by reversed-phase column chromatography, as described for compound **8**.

Yield: 9% (16 mg); yellow solid, mp 136–138 °C; Rf = 0.19 (CH_2Cl_2/MeOH = 9/1 + 0.3% NH_3 (25% aq. sol), v/v); ^{1}H NMR (400 MHz, TFA-*d*): δ 1.21–1.51 (m, 1H), 2.01–2.23 (m, 3H), 2.71–3.62 (m, 14H), 3.69–3.94 (m, 5H), 4.15–4.38 (m, 3H), 7.33 (bs, 4H), 8.19 (bs, 0.5 H), 8.44 (bs, 0.5H), 8.57–8.60 (m, 1H), 9.07 (s, 1H), 9.43 (d, *J* = 5.1 Hz, 1H), 10.32 (d, *J* = 8.7 Hz, 1H); ESI-HRMS *m/z* calcd. for $C_{29}H_{36}N_5O_4$ $[M+H]^+$ 518.2767, found 518.2782; IR (ATR) υ = 2934, 1611, 1553, 1519, 1493, 1460, 1388, 1248, 1180, 1141, 1050, 933, 789, 806, 777, 742, 703 cm^{-1}; HPLC purity, 95.5% at 254 nm (t_R = 4.81 min).

4.5.4. (±)-N-((1-(2,3-dihydro-1H-inden-2-yl)piperidin-3-yl)methyl)-N-(2-(dimethylamino)ethyl)-8-hydroxyquinoline-2-carboxamide (**11**)

Compound **11** was synthesised from 8-hydroxyquinoline-2-carboxylic acid (50 mg, 0.26 mmol, 1.0 eq.) via general procedure A. It was purified by column chromatography using CH_2Cl_2/MeOH (v/v, 20/1) + 0.3% NH_3 (25% aq. sol) as eluent.

Yield: 46% (57 mg); yellow solid, mp 68–71 °C; Rf = 0.40 (CH_2Cl_2/MeOH = 9/1 + 0.3% NH_3 (25% aq. sol), v/v); ^{1}H NMR (400 MHz, $CDCl_3$): 1.12–1.23 (m, 1H), 1.70–1.81 (m, 3H), 2.01–2.15 (m, 2H), 2.23–2.27 (m, 1H), 2.32 (s, 6H), 2.87–3.03 (m, 6H), 3.06–3.12 (m, 2H), 3.23–3.31 (m, 1H), 3.53 (dd, *J* = 13.5, 6.9 Hz, 1H), 3.61 (dd, *J* = 13.5, 8.1 Hz, 1H), 4.08–4.19 (m, 2H), 7.10–7.17 (m, 4H), 7.19 (dd, *J* = 7.7, 1.2 Hz, 1H), 7.31 (dd, *J* = 8.2, 1.2 Hz, 1H), 7.49–7.53 (m, 1H), 8.17 (d, *J* = 8.6 Hz, 1H), 8.23 (dd, *J* = 8.8 Hz, 1H), resonance for OH missing; ^{13}C NMR (100 MHz, $CDCl_3$): δ 24.82, 28.71, 35.41, 36.78, 36.92, 45.28, 48.89, 51.78, 52.01, 56.07, 59.35, 67.13, 117.02, 122.60, 124.26, 124.30, 126.37, 129.08, 129.51, 136.82, 141.31, 141.35, 149.79, 155.28, 166.05; ESI-HRMS *m/z* calcd. for $C_{29}H_{37}N_4O_2$ $[M+H]^+$ 473.2917, found 473.2909; IR (ATR) υ = 2933, 2789, 1624, 1562, 1463, 1377, 1324, 1237, 1143, 1114, 1063, 842, 744 cm^{-1}; HPLC purity, 95.8% at 254 nm (t_R = 5.18 min).

4.5.5. (±)-N-((1-(2,3-dihydro-1H-inden-2-yl)piperidin-3-yl)methyl)-N-(2-(dimethylamino)ethyl)-8-hydroxy-5-nitroquinoline-2-carboxamide (**12**)

Compound **12** was synthesised from 8-hydroxy-5-nitroquinoline-2-carboxylic acid [46] (34 mg, 0.145 mmol, 1.0 eq.) via general procedure A. It was purified by column chromatography using CH_2Cl_2/MeOH (v/v, 9/1) + 0.3% NH_3 (25% aq. sol) as eluent, and subsequently by reversed-phase column chromatography.

Yield: 52% (39 mg); yellow solid, mp 67–70 °C; Rf = 0.18 (CH_2Cl_2/MeOH = 9/1 + 0.3% NH_3 (25% aq. sol), v/v); ^{1}H NMR (400 MHz, $CDCl_3$): δ 1.27–1.39 (m, 2H), 1.88–1.98 (m, 2H), 2.19–2.27 (m, 1H), 2.53–2.66 (m, 2H), 2.83 (s, 6H), 3.20–3.45 (m, 8H), 3.72–3.80 (m, 2H), 4.06–4.13 (m, 2H), 4.75–4.83 (m, 1H), 6.77 (d, *J* = 9.4 Hz, 1H), 7.13–7.17 (m, 4H), 8.27 (d, *J* = 9.2 Hz, 1H), 8.62 (d, *J* = 9.4 Hz, 1H), 9.51 (d, *J* = 9.2 Hz, 1H), resonance for OH missing; ^{13}C NMR (100 MHz, $CDCl_3$): δ 22.37, 27.19, 29.67, 34.57, 35.08, 44.44, 47.84, 50.74, 51.68, 54.92, 58.23, 66.98, 113.27, 124.22, 124.45, 125.70, 125.90, 127.50, 127.59, 128.67, 133.64, 134.53, 138.55, 138.69, 138.83, 146.89, 165.99, 173.22; ESI-HRMS *m/z* calcd. for $C_{29}H_{36}N_5O_4$ $[M+H]^+$ 518.2767, found 518.2780; IR (ATR) υ = 3333, 2926, 1630, 1597, 1555, 1475, 1361, 1251, 1178, 1132, 1038, 980, 952, 833, 808, 758, 740 cm^{-1}; HPLC purity, 95.6% at 254 nm (t_R = 5.50 min).

4.5.6. (±)-N-((1-(2,3-dihydro-1H-inden-2-yl)piperidin-3-yl)methyl)-N-(2-(dimethylamino)ethyl)-4,8-dihydroxyquinoline-2-carboxamide (**13**)

Compound **13** was synthesised from 4,8-dihydroxyquinoline-2-carboxylic acid (100 mg, 0.49 mmol, 1.0 eq.), via general procedure

A. It was purified by column chromatography using CH_2Cl_2/MeOH (v/v, 4/1) + 0.3% NH_3 (25% aq. sol) as eluent.

Yield: 20% (47 mg); pale yellow solid, mp 78–81 °C; Rf = 0.20 (CH_2Cl_2/MeOH = 4/1 + 0.3% NH_3 (25% aq. sol), v/v); ^{1}H NMR (400 MHz, MeOD): 0.82–0.92 (m, 0.7H), 1.15–1.23 (m, 0.3H), 1.54–2.09 (m, 6H), 2.20 (bs, 3H), 2.45 (bs, 4H), 2.65–3.29 (m, 10H), 3.50–3.58 (m, 1H), 3.74–3.85 (m, 1H), 6.28–6.40 (m, 1H), 7.12–7.19 (m, 5H), 7.26–7.30 (m, 1H), 7.72 (dd, J = 8.3, 1.2 Hz, 1H), resonances for OH missing; ESI-HRMS *m/z* calcd. for $C_{29}H_{37}N_4O_3$ $[M+H]^+$ 489.2866, found 489.2878; IR (ATR) υ = 2932, 1630, 1577, 1523, 1444, 1375, 1284, 1168, 1017, 811, 745 cm^{-1}; HPLC purity, 99.3% at 254 nm (t_R = 4.39 min).

4.5.7. (±)-N-((1-(2,3-Dihydro-1H-inden-2-yl)piperidin-3-yl) methyl)-N-(2-(dimethylamino)ethyl)-6-hydroxy-2,5,7,8-tetramethylchroman-2-carboxamide (**14**)

Compound **14** was synthesised from Trolox (0.070 mg, 0.28 mmol, 1.0 eq.) via general procedure A. It was purified by column chromatography using CH_2Cl_2/MeOH (v/v, 9/1) as eluent, to obtain a mixture of four diastereoisomers and enantiomers.

Yield: 9% (14 mg); white solid, mp 45–47 °C; Rf = 0.15 (CH_2Cl_2/MeOH = 9/1, v/v); ^{1}H NMR (400 MHz, $CDCl_3$): δ 0.73–1.09 (m, 1.5H), 1.20–1.37 (m, 0.5H), 1.47–1.84 (m, 6H), 1.89–2.34 (m, 15H), 2.42–2.77 (m, 5H), 2.85–3.14 (m, 7H), 3.22–3.68 (m, 7H), 4.11–4.48 (m, 1H), 7.11–7.18 (m, 4H), resonance for OH missing; ^{13}C NMR (100 MHz, $CDCl_3$): δ 12.09, 12.36, 13.07, 21.18, 24.10, 24.52, 25.82, 27.90, 28.44, 27.90, 28.44, 29.63, 31.87, 33.97, 34.95, 35.35, 36.12, 36.49, 36.78, 45.29, 45.64, 51.41, 51.77, 55.75, 57.80, 58.08, 66.60, 67.60, 79.50, 80.84, 118.56, 122.25, 124.34, 126.53, 126.68, 138.58, 140.64, 141.15, 141.70, 148.38, 154.61, 154.93, 173.57; ESI-HRMS *m/z* calcd. for $C_{33}H_{48}N_3O_3$ $[M+H]^+$ 534.3696, found 534.3709; IR (ATR) υ = 2933, 2854, 2767, 1714, 1631, 1459, 1406, 1373, 1237, 1194, 1096, 1062, 1022, 935, 871, 743 cm^{-1}; HPLC purity (both diastereoisomers), 95.2% at 254 nm (t_R = 5.23 and 5.34 min).

4.5.8. (±)-(2 R)-N-((1-(2,3-dihydro-1H-inden-2-yl)piperidin-3-yl) methyl)-N-(2-(dimethylamino)ethyl)-4-(2-hydroxyphenyl)-2,5-dihydrothiazole-2-carboxamide (**15**)

Compound **15** was synthesised from **7a** (105 mg, 0.47 mmol, 1.0 eq.) via general procedure A. It was purified by column chromatography using CH_2Cl_2/MeOH (v/v, 20/1) + 0.3% NH_3 (25% aq. sol) as eluent.

Yield: 42% (101 mg); pale orange solid, mp 45–47 °C; Rf = 0.55 (CH_2Cl_2/MeOH = 9/1 + 0.3% NH_3 (25% aq. sol), v/v); ^{1}H NMR (400 MHz, $CDCl_3$): δ 0.98–1.09 (m, 0.7H), 1.16–1.22 (m, 0.3H), 1.57–2.09 (m, 5H), 2.27 (s, 6H), 2.42–2.67 (m, 3H), 2.77–3.49 (m, 10H), 3.65–4.12 (m, 3H), 5.48–5.71 (m, 1H), 6.76–7.06 (m, 3H), 7.10–7.21 (m, 3H), 7.23–7.48 (m, 3H); ^{13}C NMR (100 MHz, $CDCl_3$): δ 24.53, 24.69, 24.83, 28.23, 28.59, 32.28, 32.47, 32.58, 32.63, 34.86, 34.96, 36.35, 36.41, 36.79, 36.82, 36.93, 36.98, 37.09, 44.58, 45.20, 45.57, 45.60, 45.88, 46.57, 49.00, 49.72, 51.77, 51.91, 51.95, 52.15, 55.87, 56.10, 56.20, 58.01, 58.14, 66.73, 67.03, 67.07, 67.22, 75.04, 75.30, 115.98, 116.00, 116.02, 116.05, 116.89, 116.93, 116.97, 117.13, 118.63, 118.94, 118.98, 124.04, 124.26, 126.02, 126.26, 126.33, 126.40, 127.96, 128.06, 128.14, 128.23, 128.84, 129.11, 129.21, 130.80, 133.15, 133.28, 133.34, 133.39, 134.09, 141.28, 141.30, 141.32, 141.45, 141.50, 158.68, 158.77, 158.84, 168.45, 168.67, 168.78, 173.66, 173.88, 173.90, 174.03; ESI-HRMS *m/z* calcd. for $C_{29}H_{39}N_4O_2S$ $[M+H]^+$ 507.2794, found 507.2790; IR (ATR) υ = 2934, 2767, 1648, 1622, 1592, 1486, 1453, 1288, 1254, 1219, 1155, 1118, 1034, 955, 817, 745, 670 cm^{-1}; HPLC purity, 95.1% at 254 nm (t_R = 5.95 min).

4.5.9. (±)-N-((1-(2,3-dihydro-1H-inden-2-yl)piperidin-3-yl) methyl)-N-(2-(dimethylamino)ethyl)-2-(pyridin-2-ylamino) thiazole-4-carboxamide (**16**)

Compound **16** was synthesised from **7b** (80 mg, 0.36 mmol, 1.0 eq.) via general procedure A. It was purified by column chromatography using CH_2Cl_2/MeOH (v/v, 20/1) + 0.3% NH_3 (25% aq. sol) as eluent.

Yield: 48% (88 mg); pale yellow solid, mp 88–91 °C; Rf = 0.38 (CH_2Cl_2/MeOH = 9/1 + 0.3% NH_3 (25% aq. sol), v/v); ^{1}H NMR (400 MHz, $CDCl_3$): δ 0.76–1.10 (m, 1H), 1.41–1.70 (m, 3H), 1.89–2.26 (m, 9H), 2.41–3.18 (m, 8H), 3.38–3.87 (m, 5H), 6.84–6.87 (m, 2H), 7.09–7.14 (m, 4H), 7.20–7.36 (m, 1H), 7.56 (t, J = 7.3 Hz, 1H), 8.31–8.33 (m, 1H), 9.82 (bs, 1H); ^{13}C NMR (100 MHz, $CDCl_3$): δ 24.81, 28.60, 35.33, 36.13, 36.77, 37.05, 44.99, 45.56, 46.84, 50.05, 51.95, 52.85, 55.43, 56.18, 56.41, 57.90, 63.39, 67.09, 110.58, 115.5, 116.09, 116.40, 124.29, 126.30, 128.09, 129.18, 137.78, 141.27, 141.55, 144.85, 146.65, 151.30, 159.40, 159.54, 165.05, 165.58; ESI-HRMS *m/z* calcd. for $C_{28}H_{37}N_6OS$ $[M+H]^+$ 505.2750, found 505.2760; IR (ATR) υ = 2932, 1605, 1537, 1479, 1455, 1409, 1305, 1223, 1150, 1053, 773, 741, 660 cm^{-1}; HPLC purity, 95.3% at 254 nm (t_R = 5.26 min).

4.5.10. (±)-N-((1-(2,3-dihydro-1H-inden-2-yl)piperidin-3-yl) methyl)-N-(2-(dimethylamino)ethyl)-8-hydroxyimidazo[1,2-a] pyridine-2-carboxamide (**17**)

Compound **17** was synthesised from **7c** (71 mg, 0.40 mmol, 1.0 eq.) via general procedure A. The residue was purified by column chromatography using CH_2Cl_2/MeOH (v/v, 9/1) + 0.3% NH_3 (25% aq. sol) as eluent, and subsequently by reversed-phase column chromatography.

Yield: 48% (75 mg); brown solid, mp 105–107 °C; Rf = 0.09 (CH_2Cl_2/MeOH = 9/1 + 0.3% NH_3 (25% aq. sol), v/v); ^{1}H NMR (400 MHz, $CDCl_3$): δ 1.04–1.14 (m, 1H), 1.55–1.81 (m, 3H), 1.90–2.12 (m, 2H), 2.19–2.42 (m, 7H), 2.57–2.62 (m, 1H), 2.72–2.84 (m, 2H), 2.90–3.21 (m, 6H), 3.41–3.62 (m, 3H), 4.19–4.33 (m, 1H), 6.53–6.65 (m, 2H), 7.04–7.11 (m, 4H), 7.51–7.60 (m, 1H), 7.90–8.03 (m, 1H), 9.40 (bs, 1H); ^{13}C NMR (100 MHz, $CDCl_3$): δ 24.81, 28.63, 29.62, 31.36, 35.37, 35.66, 36.42, 36.65, 36.95, 44.65, 45.22, 45.48, 46.22, 50.45, 51.67, 51.93, 52.17, 56.16, 56.42, 57.68, 66.63, 67.15, 105.37, 106.06, 114.72, 115.57, 116.19, 116.77, 117.42, 124.28, 126.27, 126.67, 138.92, 140.36, 141.12, 141.43, 148.80, 162.47, 164.40, 165.14; ESI-HRMS *m/z* calcd. for $C_{27}H_{36}N_5O_2$ $[M+H]^+$ 462.2869, found 462.2860; IR (ATR) υ = 2932, 1612, 1537, 1458, 1294, 1241, 1159, 1048, 927, 734 cm^{-1}; HPLC purity, 95.7% at 254 nm (t_R = 4.47 min).

4.5.11. (±)-N-((1-(2,3-dihydro-1H-inden-2-yl)piperidin-3-yl) methyl)-N-(2-(dimethylamino)ethyl)-6-hydroxynicotinamide (**18**)

Compound **18** was synthesised from 6-hydroxynicotinic acid (100 mg, 0.72 mmol, 1.0 eq.) via general procedure A. It was purified by column chromatography using CH_2Cl_2/MeOH (v/v, 4/1) + 0.3% NH_3 (25% aq. sol) as eluent, and subsequently by reversed-phase column chromatography.

Yield: 13% (39 mg); orange solid, mp 60–63 °C; Rf = 0.17 (CH_2Cl_2/MeOH = 4/1 + 0.3% NH_3 (25% aq. sol), v/v); ^{1}H NMR (400 MHz, $CDCl_3$): δ 0.81–1.01 (m, 1H), 1.55–1.81 (m, 4H), 1.97–2.29 (m, 9H), 2.40–2.52 (m, 2H), 2.77–2.94 (m, 4H), 3.01–3.09 (m, 3H), 3.30–3.40 (m, 2H), 3.45–3.55 (m, 2H), 6.57 (d, J = 9.4 Hz, 1H), 7.11–7.18 (m, 4H), 7.51 (d, J = 9.1 Hz, 1H), 7.59 (bs, 1H); ^{13}C NMR (100 MHz, $CDCl_3$): δ 24.58, 28.39, 35.06, 36.57, 36.80, 45.60, 51.79, 55.37, 56.98, 66.80, 116.32, 119.90, 124.26, 124.32, 126.42, 135.23, 140.93, 141.29, 141.34, 164.65, 168.53; ESI-HRMS *m/z* calcd. for $C_{25}H_{35}N_4O_2$ $[M+H]^+$ 423.2760, found 423.2770; IR (ATR) υ = 2933, 2791, 1654, 1613, 1544, 1427, 1348, 1213, 1132, 1042, 932, 838, 744, 659 cm^{-1}; HPLC purity, 98.4% at 254 nm (t_R = 3.71 min).

*4.5.12. (±)-N-((1-(2,3-dihydro-1H-inden-2-yl)piperidin-3-yl) methyl)-N-(2-(dimethylamino)ethyl)-2-oxo-2H-chromene-3-carboxamide (**19**)*

A solution of 2-oxo-2*H*-chromene-3-carboxylic acid (323 mg, 1.70 mmol, 3.4 eq.) in $SOCl_2$ (8 mL) was stirred under an argon atmosphere at 80 °C for 4 h. The reagent was evaporated under reduced pressure, and the oily residue was dried under vacuum for 30 min. Anhydrous pyridine (10 mL) was added under an argon atmosphere to dissolve the acyl chloride formed. A solution of **5** [15] (323 mg, 0.50 mmol, 1.0 eq.) in anhydrous pyridine (5 mL) was then added, and the mixture was stirred at room temperature for 72 h. The solvent was evaporated, and the residue was dissolved in CH_2Cl_2 (100 mL) and transferred into a separating funnel. The organic phase was washed with saturated aqueous $NaHCO_3$ solution (2 × 70 mL), and saturated brine solution (100 mL), dried over anhydrous Na_2SO_4, filtered, and evaporated under reduced pressure. The residue was purified by reversed-phase column chromatography (Isolera Biotage system, SNAP Biotage KP-18-HS column) using a gradient of 0.1% TFA (aq) and MeCN as eluent. The fractions containing the product were combined and the organic solvent was evaporated under reduced pressure. The remaining aqueous solution was made alkaline using saturated aqueous solution of $NaHCO_3$ (80 mL), transferred into a separating funnel, and extracted with CH_2Cl_2 (3 × 50 mL). The combined organic phases were dried over anhydrous Na_2SO_4, filtered, and evaporated under reduced pressure.

Yield: 19% (44 mg); white solid, mp 88–91 °C; Rf = 0.10 (CH_2Cl_2/MeOH = 9/1); ^{1}H NMR (400 MHz, $CDCl_3$): δ 0.76–0.89 (m, 0.4H), 1.09–1.20 (m, 0.6H), 1.67–2.14 (m, 7H), 2.20–2.26 (m, 1H), 2.34 (s, 2H), 2.40–2.47 (m, 1.3H), 2.62–2.66 (m, 0.7H), 2.81–3.65 (m, 12H), 2.57–2.66 (m, 1H), 7.11–7.21 (m, 4H), 7.29–7.34 (m, 1H), 7.36–7.38 (m, 1H), 7.47–7.53 (m, 1H), 7.56–7.61 (m, 1H), 7.75 (s, 0.4H), 7.82 (s, 0.6H); ^{13}C NMR (100 MHz, $CDCl_3$): δ 24.62, 28.24, 28.44, 34.44, 35.34, 36.59, 36.80, 36.94, 43.59, 45.64, 45.71, 46.58, 47.81, 51.87, 52.03, 53.13, 55.68, 56.14, 57.60, 66.97, 67.35, 116.84, 118.20, 118.27, 124.29, 124.32, 124.38, 124.49, 124.85, 125.81, 125.99, 126.38, 126.45, 128.32, 128.46, 132.57, 132.63, 141.34, 141.89, 142.10, 153.94, 157.94, 158.06, 165.32, 165.72; ESI-HRMS *m/z* calcd. for $C_{29}H_{36}N_3O_3$ $[M+H]^+$ 474.2757, found 474.2750; IR (ATR) υ = 2931, 2823, 2772, 1709, 1631, 1607, 1573, 1466, 1434, 1365, 1306, 1255, 1201, 1171, 1118, 1018, 948, 825, 753, 738, 702 cm^{-1}; HPLC purity, 95.2% at 254 nm (t_R = 5.17 min).

*4.5.13. (E)-4-(3-(((1-(2,3-dihydro-1H-inden-2-yl)piperidin-3-yl) methyl) (2-(dimethylamino)ethyl)amino)-3-oxoprop-1-en-1-yl) phenyl acetate (**20**)*

Compound **20** was synthesised from 4-acetoxycinnamic acid (206 mg, 1.0 mmol, 1.0 eq.) via general procedure B, and was used in the following reaction step as a crude material.

Yield: 11%; off-white solid, Rf = 0.42 (EtOAc/MeOH = 3/1, v/v); ^{1}H NMR (400 MHz, $CDCl_3$): δ 0.95–1.14 (m, 1H), 1.52–1.79 (m, 4H), 1.91–2.11 (m, 4H), 2.18 (s, 3H), 2.31 (s, 3H), 2.36 (s, 3H), 2.51–2.65 (m, 2H), 2.84–3.32 (m, 7H), 3.46–3.57 (m, 1.6H), 3.64–3.72 (m, 0.4H), 6.37 (d, J = 15.5 Hz, 0.6H), 6.65–6.75 (m, 2.4H), 7.09–7.17 (m, 4H), 7.21 (d, J = 8.3 Hz, 1.2H), 7.33 (d, J = 8.3 Hz, 0.8H), 7.48 (d, J = 15.3 Hz, 0.6H), 7.62 (d, J = 15.3 Hz, 0.4H); ESI-MS *m/z* calcd. for $C_{30}H_{40}N_3O_3$ $[M+H]^+$ 490.31, found 490.20.

*4.5.14. (±)-3-(((1-(2,3-dihydro-1H-inden-2-yl)piperidin-3-yl) methyl) (2-(dimethylamino)ethyl) carbamoyl)phenyl acetate (**21**)*

Compound **21** was synthesised from 3-acetoxybenzoic acid (250 mg, 1.39 mmol, 1.0 eq.) via general procedure B.

Yield: 79% (455 mg); orange oil, Rf = 0.24 (CH_2Cl_2/MeOH = 15/1, v/v); ^{1}H NMR (400 MHz, $CDCl_3$): δ 0.65–0.75 (m, 0.4H), 1.11–1.18 (m, 0.6H), 1.41–1.95 (m, 5H), 2.03 (s, 3H), 2.09–2.14 (m, 1H), 2.23–2.37 (m, 7H), 2.57 (bs, 1H), 2.77–3.66 (m, 11H), 7.07–7.23 (m, 7H), 7.37–7.43 (m, 1H); ESI-HRMS *m/z* calcd. for $C_{28}H_{38}N_3O_3$ $[M+H]^+$ 464.2913, found 464.2909.

*4.5.15. (±)-4-(((1-(2,3-dihydro-1H-inden-2-yl)piperidin-3-yl) methyl) (2-(dimethylamino)ethyl) carbamoyl)phenyl acetate (**22**)*

Compound **22** was synthesised from 4-acetoxybenzoic acid (250 mg, 1.39 mmol, 1.0 eq.) via general procedure B.

Yield: 48% (276 mg); brown solid, mp 49–51, Rf = 0.24 (CH_2Cl_2/MeOH = 15/1, v/v); ^{1}H NMR (400 MHz, $CDCl_3$): δ 0.64–0.75 (m, 0.4H), 1.03–1.16 (m, 0.6H), 1.38–1.91 (m, 5H), 2.02 (s, 3H), 2.08–2.13 (m, 1H), 2.21–2.39 (m, 7H), 2.57 (bs, 1H), 2.73–3.66 (m, 11H), 7.10–7.18 (m, 6H), 7.31–7.36 (m, 2H); ESI-HRMS *m/z* calcd. for $C_{28}H_{38}N_3O_3$ $[M+H]^+$ 464.2913, found 464.2917.

*4.5.16. (±)-4-(((1-(2,3-dihydro-1H-inden-2-yl)piperidin-3-yl) methyl) (2-(dimethylamino)ethyl) carbamoyl)-1,3-phenylene diacetate (**23**)*

Compound **23** was synthesised from 2,4-diacetoxybenzoic acid (250 mg, 1.05 mmol, 1.0 eq.) via general procedure B, and was used in the following reaction step as a crude material.

Yield: 79% (165 mg); orange oil, Rf = 0.30 (CH_2Cl_2/MeOH = 9/1, v/v); ^{1}H NMR (400 MHz, $CDCl_3$): δ 0.67–0.73 (m, 0.4H), 1.09–1.18 (m, 0.6H), 1.54–1.99 (m, 5H), 2.05 (s, 3H), 2.03–2.13 (m, 1H), 2.23–2.25 (m, 3H), 2.28–2.36 (m, 7H), 2.55–2.59 (m, 1H), 2.81–3.42 (m, 11H), 7.00–7.06 (m, 2H), 7.10–7.33 (m, 5H); ESI-MS *m/z* calcd. for $C_{30}H_{40}N_3O_5$ $[M+H]^+$ 522.30, found 522.15.

*4.5.17. (±)-((E)-N-((1-(2,3-dihydro-1H-inden-2-yl)piperidin-3-yl) methyl)-N-(2-(dimethylamino)ethyl)-3-(4-hydroxyphenyl) acrylamide (**24**)*

Compound **24** was synthesised from **20** via general procedure C.

Yield: 38% (18 mg); slightly yellow crystals, mp 67–70 °C; Rf = 0.47 (CH_2Cl_2/MeOH = 9/1 + 0.3% NH_3 (25% aq. sol), v/v); ^{1}H NMR (400 MHz, $CDCl_3$): δ 0.83–1.10 (m, 1H), 1.51–1.86 (m, 4H), 2.00–2.08 (m, 4H), 2.29 (s, 3H), 2.35 (s, 3H), 2.50–2.63 (m, 2H), 2.80–3.30 (m, 7H), 3.45–3.55 (m, 1.6H), 3.62–3.70 (m, 0.4H), 5.92 (bs, 1H), 6.41 (d, J = 15.3 Hz, 0.6H), 6.66 (d, J = 15.2 Hz, 0.4H), 6.69 (d, J = 8.3 Hz, 1.2H), 6.75 (d, J = 8.2 Hz, 0.8H), 7.07–7.17 (m, 4H), 7.22 (d, J = 8.3 Hz, 1.2H), 7.34 (d, J = 8.2 Hz, 0.8H), 7.51 (d, J = 15.2 Hz, 0.6H), 7.62 (d, J = 15.2 Hz, 0.4H); ^{13}C NMR (100 MHz, $CDCl_3$): δ 24.42, 24.64, 28.55, 28.63, 29.19, 35.76, 36.12, 36.48, 36.74, 36.87, 44.86, 45.31, 45.55, 46.21, 50.26, 51.50, 51.93, 55.67, 56.24, 56.68, 58.11, 67.08, 67.15, 113.16, 113.30, 116.02, 116.14, 124.31, 126.39, 126.45, 129.69, 129.74, 141.24, 141.29, 142.77, 143.52, 158.96, 159.15, 167.29, 167.46; ESI-HRMS *m/z* calcd. for $C_{28}H_{38}N_3O_2$ $[M+H]^+$ 448.2964, found 448.2954; IR (ATR) υ = 2935, 2794, 1639, 1583, 1513, 1448, 1373, 1318, 1279, 1239, 1167, 1118, 1041, 978, 937 cm^{-1}; HPLC purity, 95.2% at 254 nm (t_R = 4.71 min).

*4.5.18. (±)-N-((1-(2,3-dihydro-1H-inden-2-yl)piperidin-3-yl) methyl)-N-(2-(dimethylamino)ethyl)-3-hydroxybenzamide (**25**)*

Compound **25** was synthesised from compound **21** via general procedure C.

Yield: 77% (288 mg); brown oil; Rf = 0.08 (CH_2Cl_2/MeOH = 9/1); ^{1}H NMR (400 MHz, $CDCl_3$): δ 0.64–0.73 (m, 0.4H), 1.07–1.15 (m, 0.6H), 1.44–2.14 (m, 10H), 2.30–2.37 (m, 3H), 2.60–2.65 (m, 1H), 2.75–3.66 (m, 11H), 6.71–6.80 (m, 3H), 7.12–7.19 (m, 5H), resonance for OH missing; ^{13}C NMR (100 MHz, $CDCl_3$): δ 24.35, 28.22, 34.84, 35.00, 36.16, 36.49, 42.76, 44.98, 45.15, 46.71, 48.12, 51.50, 53.18, 53.29, 55.35, 55.81, 56.04, 57.13, 66.74, 66.87, 113.62, 114.04, 116.77, 117.46, 124.11, 124.15, 126.24, 129.47, 137.18, 140.99, 141.03, 157.02, 157.16, 172.39, 172.57; ESI-HRMS *m/z* calcd. for $C_{26}H_{36}N_3O_2$ $[M+H]^+$ 422.2808, found 422.2798; IR (ATR) υ = 2935, 2791, 1580, 1444, 1349, 1291, 1228, 1159, 1130, 1110, 1043, 876, 792, 744,

700 cm^{-1}; HPLC purity, 96.1% at 254 nm (t_R = 4.40 min).

*4.5.19. (±)-N-((1-(2,3-dihydro-1H-inden-2-yl)piperidin-3-yl) methyl)-N-(2-(dimethylamino)ethyl)-4-hydroxybenzamide (**26**)*

Compound **26** was synthesised from compound **22** via general procedure C. It was purified by column chromatography using CH_2Cl_2/MeOH (v/v, 9/1) as eluent.

Yield: 65% (114 mg); orange solid, mp 47–51 °C; Rf = 0.11 (CH_2Cl_2/MeOH = 9/1); ^{1}H NMR (400 MHz, $CDCl_3$): δ 0.67 (bs, 0.4H), 1.09 (bs, 0.6H), 1.44–2.41 (m, 13H), 2.62 (bs, 1H), 2.77–3.69 (m, 11H), 6.62 (d, J = 7.8 Hz, 2H), 7.09–7.16 (m, 6H), resonance for OH missing; ^{13}C NMR (100 MHz, $CDCl_3$): δ 24.50, 28.38, 35.15, 36.59, 43.19, 45.29, 47.27, 48.47, 51.68, 53.68, 55.47, 56.00, 56.42, 57.23, 66.95, 115.47, 124.26, 126.37, 126.67, 128.31, 128.65, 141.15, 141.21, 158.44, 173.09; ESI-HRMS *m/z* calcd. for $C_{26}H_{36}N_3O_2$ $[M+H]^+$ 422.2808, found 422.2799; IR (ATR) υ = 2935, 2791, 1607, 1515, 1425, 1372, 1275, 1166, 1135, 1105, 1044, 910, 843, 729 cm^{-1}; HPLC purity, 97.6% at 254 nm (t_R = 4.26 min).

*4.5.20. (±)-N-((1-(2,3-dihydro-1H-inden-2-yl)piperidin-3-yl) methyl)-N-(2-(dimethylamino)ethyl)-2,4-dihydroxybenzamide (**27**)*

Compound **27** was synthesised from compound **23** via general procedure C.

Yield: 38% (49 mg); pale brown solid, mp 87–89 °C; Rf = 0.05 (CH_2Cl_2/MeOH = 9/1); ^{1}H NMR (400 MHz, $CDCl_3$): δ 0.83 (bs, 1H), 1.53–1.77 (m, 4H), 1.91–2.04 (m, 2H), 2.27 (bs, 6H), 2.52 (bs, 2H), 2.85–3.29 (m, 9H), 3.58–3.82 (m, 2H), 6.18 (dd, J = 8.4, 1.9 Hz, 1H), 6.30 (s, 1H), 6.97 (d, J = 8.3 Hz, 1H), 7.10–7.17 (m, 4H), resonance for OH missing; ^{13}C NMR (100 MHz, $CDCl_3$): δ 24.35, 28.22, 34.84, 35.00, 36.16, 36.49, 42.76, 44.98, 45.15, 46.71, 48.12, 51.50, 53.18, 53.29, 55.35, 55.81, 56.04, 57.13, 66.74, 66.87, 113.62, 114.04, 116.77, 117.46, 124.11, 124.15, 126.24, 129.47, 137.18, 140.99, 141.03, 157.02, 157.16, 172.39, 172.57; ESI-HRMS *m/z* calcd. for $C_{26}H_{36}N_3O_3$ $[M+H]^+$ 438.2757, found 438.2751; IR (ATR) υ = 2932, 1597, 1429, 1349, 1305, 1259, 1220, 1171, 1101, 1045, 977, 909, 844, 810, 742 cm^{-1}; HPLC purity, 95.7% at 254 nm (t_R = 4.08 min).

*4.5.21. (±)-N-((1-(2,3-dihydro-1H-inden-2-yl)piperidin-3-yl) methyl)-N-(2-(dimethylamino)ethyl)-4-methoxybenzamide (**28**)*

To a solution of **5** [15] (400 mg, 0.62 mmol, 1.0 eq.) and Et_3N (345 μL, 2.48 mmol, 4.0 eq.) in CH_2Cl_2 (50 mL) cooled to 0 °C, 4-methoxybenzoyl chloride (400 mg, 0.74 mmol, 1.2 eq.) was added, and the mixture was stirred at room temperature for 16 h. Then the mixture was transferred into the separating funnel and CH_2Cl_2 (30 mL) was added. Organic phase was washed with saturated aqueous solutions of $NaHCO_3$ (30 mL), water (30 mL) and saturated brine solution (30 mL), dried over anhydrous Na_2SO_4, filtered, and evaporated under reduced pressure. The residue was purified by column chromatography using CH_2Cl_2/MeOH (v/v, 20/1) as eluent.

Yield: 16% (42 mg); orange oil; Rf = 0.20 (CH_2Cl_2/MeOH = 15/1, v/v); ^{1}H NMR (400 MHz, $CDCl_3$): δ 0.68 (bs, 0.4H), 1.10 (bs, 0.6H), 1.37–2.44 (m, 13H), 2.53–3.61 (m, 12H), 3.81 (s, 3H), 6.88 (d, J = 8.2 Hz, 2H), 7.11–7.18 (m, 4H), 7.29 (bs, 2H); ^{13}C NMR (100 MHz, $CDCl_3$): δ 24.78, 28.50, 35.30, 36.84, 43.25, 45.54, 47.40, 48.29, 51.94, 53.63, 55.24, 55.59, 55.99, 56.75, 57.53, 67.02, 113.61, 124.27, 124.30, 126.35, 128.42, 129.01, 141.36, 141.41, 160.20, 172.22; ESI-HRMS *m/z* calcd. for $C_{27}H_{38}N_3O_2$ $[M+H]^+$ 436.2964, found 436.2961; IR (ATR) υ = 2934, 2768, 1609, 1512, 1460, 1424, 1348, 1299, 1248, 1173, 1135, 1110, 1027, 936, 840, 799, 744 cm^{-1}; HPLC purity, 95.6% at 254 nm (t_R = 4.92 min).

*4.5.22. (±)-N-(2-(dimethylamino)ethyl)-N-((1-((2-(pyridin-2-ylamino)thiazol-4-yl)methyl)piperidin-3-yl)methyl)-2-naphthamide (**29**)*

Amine **6b** (231 mg, 0.68 mmol, 1.0 eq.), alkyl chloride **7d** (178 mg, 0.68 mmol, 1.0 eq., see Supporting Information) and K_2CO_3 (282 mg, 2.04 mmol, 3.0 eq.) were suspended in anhydrous DMF (7 mL), and stirred under an argon atmosphere at 50 °C for 16 h. The solvent was evaporated, and the residue was dissolved in CH_2Cl_2 (60 mL) and transferred into a separating funnel. The organic phase was washed with saturated aqueous $NaHCO_3$ solution (2 × 50 mL) and saturated brine solution (50 mL), dried over anhydrous Na_2SO_4, filtered, and evaporated under reduced pressure. The residue was purified by column chromatography using CH_2Cl_2/MeOH (v/v, 9/1) + 0.3% NH_3 (25% aq. sol) as eluent, and subsequently by reversed-phase column chromatography (Isolera Biotage system, SNAP Biotage KP-18-HS column; gradient: 0.1% TFA (aq) and MeCN). The fractions containing the product were combined and treated as described in general procedure A.

Yield: 8% (30 mg); pale organge solid, mp 115–118 °C; Rf = 0.19 (CH_2Cl_2/MeOH = 9/1 + 0.3% NH_3 (25% aq. sol), v/v); ^{1}H NMR (400 MHz, $CDCl_3$): δ 0.60–0.68 (m, 0.4H), 1.17–1.22 (m, 0.6H), 1.41–1.70 (m, 3H), 1.52–2.07 (m, 7H), 2.18–2.56 (m, 5H), 2.84–3.08 (m, 2H), 3.29–3.58 (m, 6H), 6.58–6.88 (m, 3H), 7.31–7.57 (m, 4H), 7.74–7.87 (m, 4H), 8.35 (d, J = 4.7 Hz, 1H); ^{13}C NMR (100 MHz, $CDCl_3$): δ 24.51, 28.21, 28.35, 28.42, 34.79, 35.20, 42.98, 45.47, 47.18, 47.96, 53.40, 53.86, 54.51, 56.52, 57.22, 57.67, 58.82, 108.75, 109.23, 110.34, 116.11, 123.96, 124.40, 125.77, 126.45, 126.64, 127.68, 128.13, 128.21, 128.25, 132.57, 133.24, 134.14, 137.59, 146.82, 147.13, 151.41, 160.00, 172.31; ESI-HRMS *m/z* calcd. for $C_{30}H_{37}N_6OS$ $[M+H]^+$ 529.2750, found 529.2768; IR (ATR) υ = 2932, 2770, 1604, 1537, 1479, 1451, 1409, 1326, 1304, 1149, 1099, 1048, 996, 864, 822, 773, 755, 737, 667 cm^{-1}; HPLC purity, 96.5% at 254 nm (t_R = 4.55 min).

*4.5.23. (±)-N-(2-(dimethylamino)ethyl)-N-((1-((8-hydroxyquinolin-2-yl)methyl)piperidin-3-yl)methyl)-2-naphthamide (**30**)*

Amine **6b** (300 mg, 0.88 mmol, 1.0 eq.) was dissolved in $ClCH_2CH_2Cl$ (15 mL) and stirred and agitated with a stream of argon for 10 min. AcOH (50 μL, 0.88 mmol, 1.0 eq.), $NaBH(OAc)_3$ (560 mg, 2.64 mmol, 3.0 eq.) and 8-hydroxyquinoline-2-carboxyaldehyde (168 mg, 0.96 mmol, 1.1 eq.) were added, and the resulting suspension was stirred under an argon atmosphere at room temperature for 24 h. The reaction mixture was quenched with saturated aqueous $NaHCO_3$ solution, and the solvent was evaporated under reduced pressure. The residue was dissolved in CH_2Cl_2 (50 mL) and transferred into a separating funnel. The organic phase was washed with saturated aqueous $NaHCO_3$ solution (50 mL) and saturated brine solution (50 mL), dried over anhydrous Na_2SO_4, filtered, and evaporated under reduced pressure. The residue was purified by column chromatography using CH_2Cl_2/MeOH (v/v, 9/1) + 0.3% NH_3 (25% aq. sol) as eluent, and subsequently by reversed-phase column chromatography (Isolera Biotage system, SNAP Biotage KP-18-HS column; gradient: 0.1% TFA (aq) and MeCN). The fractions containing the product were combined and treated as described in general procedure A.

Yield: 27% (116 mg); orange solid, mp 44–46 °C; Rf = 0.25 (CH_2Cl_2/MeOH = 9/1 + 0.3% NH_3 (25% aq. sol), v/v); ^{1}H NMR (400 MHz, $CDCl_3$): δ 0.67–0.75 (m, 0.4H), 1.12–1.22 (m, 0.6H), 1.43–2.33 (m, 13H), 2.54–2.72 (m, 2H), 2.81–2.93 (m, 1H), 3.18–3.90 (m, 6H), 7.15–6.17 (m, 1H), 7.23–7.48 (m, 6H), 7.65–7.87 (m, 4H), 7.96–8.09 (m, 1H), 8.34 (bs, 1H); ^{13}C NMR (100 MHz, $CDCl_3$): δ 24.38, 24.72, 27.87, 28.26, 34.84, 35.15, 42.86, 45.40, 45.54, 47.39, 48.07, 53.04, 53.80, 54.53, 56.55, 57.53, 57.77, 65.01, 109.96, 117.49, 121.51, 121.83, 123.85, 124.31, 125.73, 126.30, 126.43, 126.64, 127.05, 127.37, 127.62, 128.09, 132.45, 133.17, 134.03, 136.24, 137.35, 151.99, 157.13, 157.38, 172.01, 172.17; ESI-HRMS *m/z* calcd. for $C_{33}H_{37}N_4O_2$ $[M+H]^+$ 497.2917, found 497.2903; IR (ATR) υ = 2934, 2820, 1621, 1572, 1504, 1471, 1429, 1369, 1323, 1243, 1193, 1135, 1099, 1048, 906, 863, 823, 752, 726 cm^{-1}; HPLC purity, 93.9% at

254 nm ($t_R = 5.42$ min).

4.6. Inhibition of cholinesterases

The inhibitory potencies of the MTDLs against the ChEs were determined using the method of Ellman following the procedure described previously [37]. Briefly, compound stock solutions (100% in DMSO) were incubated with Ellman's reagent and the ChEs (final concentrations, 333 μM Ellman's reagent, 1 nM or 50 pM hBChE or hAChE, respectively, in 0.1 M phosphate buffer, pH 8.0) for 5 min at room temperature. The reactions were started by addition of the substrate (final concentration, 500 μM butyrylthiocholine iodide/acetylthiocholine iodide). The final content of DMSO was always 1%. The increase in absorbance at 412 nm was monitored for 1 min using a 96-well microplate reader (Synergy H4; BioTek Instruments, Inc., USA). The initial velocities in the presence (v_i) and absence (v_o) of the test compounds were calculated. The inhibitory potencies are expressed as the residual activities, according to Equation (1):

$$RA = (v_i - b) / (v_o - b) \quad (1)$$

where b is the blank value using phosphate buffer instead of the ChEs. For IC_{50} determinations, at least seven different concentrations of each compound were used. The IC_{50} values were obtained by plotting the residual ChE activities against the applied inhibitor concentrations, with the experimental data fitted to a four-parameter logistic function. For the fitting procedure, the Gnuplot software and an in-house python script were used. Tacrine was used as the positive control.

4.7. DPPH radical-scavenging potency

Free-radical scavenging potency was evaluated using the DPPH assay. DPPH (2,2-diphenyl-1-picrylhydrazyl radical) was dissolved in EtOH (150 μL, 140 μM) and added to 150 μL ethanol solution of the test sample (seven concentrations, 35–5600 μM) or ethanol (negative control). The microtiter plate was shaken for 1 min and then left to stand at room temperature in the dark for 90 min. The absorbance was then determined with a microplate reader, at 517 nm (Synergy H4 Hybrid Multi-Mode Microplate Reader; BioTek). The experiments were performed in triplicate, with subtraction of the blank value (compound without DPPH). The percentages of DPPH free radicals were calculated using Equation (2):

$$\text{DPPH free radicals } (\%) = ((A_0 - A_1) / A_0) \times 100 \quad (2)$$

where A_0 is the absorbance of the negative control, and A_1 is the absorbance of the test sample. The free-radical scavenging potency is expressed as the concentration that scavenged 50% of the DPPH free radicals (EC_{50}) ± SEM. Resveratrol and Trolox were used as the positive controls under the same assay conditions.

4.8. Crystallisation, and data collection and processing

Human BChE was expressed in CHO cells, purified and concentrated to 6.0 mg/mL, as described previously [71]. The crystals of compound **11** in complex with hBChE were obtained by the co-crystallisation method. Briefly, 500 μM aqueous solution of **11** (1% DMSO) was incubated with hBChE solution (90 μM) for 3 h. Co-crystals were grown at 20 °C over a period of 3 weeks, using the hanging-drop vapour diffusion method. The mother liquor solution was 0.1 M Tris (pH 8.9), 2.3 M ammonium sulphate. Prior to data collection, crystals were cryoprotected by soaking in mother liquor solution containing 18% glycerol and compound **11** at 500 μM, before being flash-cooled directly under a stream of nitrogen at 100 K. Diffraction data were collected at the ID30A-3 (MASSIF-3) beamline of the European Synchrotron Radiation Facility (Grenoble, France) using a wavelength of 0.9679 Å. The data were indexed and integrated and processed as reported previously [15]. The protein structure was deposited in the Protein Data Bank under accession code 6F7Q.

4.9. Metal-chelating properties

The chelation properties were determined in 20 mM HEPES buffer (pH 7.4, 150 mM NaCl) using a 0.5-cm quartz cuvette and a UV–visible spectrophotometer (Varian Cary 100 Bio; Agilent, Santa Clara, CA, USA). Equimolar concentrations of $CuCl_2$, $ZnCl_2$, $CoCl_2$, $MgCl_2$, $NiCl_2$, $CaCl_2$, $MnCl_2$, $FeCl_2$, $FeCl_3$ and $AlCl_3$ were added to 30 μM compound solutions (final content, 1% DMSO). The stock solution of $FeCl_2$ was prepared in the presence of 1 mM ascorbic acid to prevent oxidation of Fe^{2+}. Chelation was detected as changes in the absorption spectra after 5 min of incubation. To further investigate the metal-ion selectivity of the test compounds for Cu^{2+} over other metal ions, a $CuCl_2$ stock solution was added to a final concentration of 30 μM. The resulting solutions that contained equimolar concentrations of the compounds, Cu^{2+}, and the various metal salts (e.g. $ZnCl_2$) were mixed, and the absorption spectra were recorded after an additional 5 min of incubation at room temperature. The selectivity was confirmed by comparing the absorbance spectra changes of the metal–ligand complexes in the presence and absence of $CuCl_2$.

The Cu^{2+}-binding stoichiometry was resolved by titration of 30 μM buffered solutions of compounds **8** and **11** with $CuCl_2$ buffered stock solutions of suitable concentrations. The absorption spectra of the compounds in the absence and presence of Cu^{2+} were recorded after 10 min incubation at room temperature. In the case of Cu^{2+} chelation, a specific change in absorbance spectra was observed. The absorbance differences at specified wavelengths (in the absence and presence of the different equivalents of Cu^{2+}) were plotted against the Cu^{2+}/**8** or Cu^{2+}/**11** molar ratios, respectively. The curves were approximated using data points at the lowest and highest Cu^{2+}/compound ratios, and the intercepts were calculated.

4.10. Ascorbate studies

The copper-ascorbate assay was performed following the literature procedure [72]. Compounds **8** and **11** (both in the form of salts with hydrochloric acid), and clioquinol, 8-hydroxyquinoline and nitroxoline (as positive controls) were dissolved in MeOH (40 mM) and diluted to 4 mM in 20 mM phosphate buffer (pH 7.4, 100 mM NaCl, 2 μM desferryl). Stock solutions of CCA and ascorbic acids were prepared in phosphate buffer, except $CuCl_2$, which was dissolved and diluted in Milli-Q water. The final sample volumes of 300 μL contained (in order of addition; final concentrations): 200 μM CCA, 40 μM compound/positive control (0.1% [v/v] MeOH), 20 μM Cu^{2+} and 600 μM ascorbate. Hydroxyl radical production was followed by measuring the conversion of CCA into 7-hydroxy-CCA (λ_{exc}, 395 nm; λ_{em}, 450 nm) using a 96-well microplate reader (Synergy H4; BioTek Instruments, Inc., USA). Experiments were performed in triplicate, and the means were used in the data analysis.

4.11. Cell based assays

4.11.1. Cell culture and treatments

The human neuroblastoma SH-SY5Y cells line was purchased from American Type Culture Collection (CRL-2266, Manassas, VA, USA). The cells were cultured in Dulbecco's modified Eagle's

medium (Sigma, St. Louis, MO, USA) supplemented with 10% foetal bovine serum (HyClone, Logan, UT, USA), 2 mM L-glutamine (Sigma, St. Louis, MO, USA), 50 U/mL penicillin and 50 μg/mL streptomycin (Sigma, St. Louis, MO, USA), in a humidified atmosphere of 95% air and 5% CO_2 at 37 °C, and grown to 80% confluence. Prior to cell treatment, complete medium was replaced with reduced-serum medium (i.e., with 2% foetal bovine serum). Compounds **8** and **11** were prepared as stock solutions at 20 mM in DMSO. For the cytotoxic stimuli, the $A\beta_{1-42}$ peptide (Merck Millipore, Darmstadt, Germany) was dissolved in DMSO to a 1 mM stock solution.

4.11.2. Cell viability assay

SH-SY5Y cells were seeded in 96-well plates (2×10^4/well) and assessed for their responses to compounds **8** and **11** using the MTS assay. The cells were treated with increasing concentrations of compounds **8** and **11** (0.5–50 μM), and cell viability was determined after 48 h using the CellTiter 96 Aqueous One Solution Cell Proliferation Assay (Promega, Madison, WI, USA), in accordance with the manufacturer instructions. Absorbance was measured with an automatic microplate reader (Tecan Safire^2, Switzerland) at a wavelength of 492 nm. Cells were treated in quadruplicate. The LD_{50} values are the mean ± SD of at least three independent experiments.

4.11.3. Neuroprotection assay

The neuroprotective effects of compounds **8** and **11** on the cytotoxic effects of $A\beta_{1-42}$ were determined using the MTS assay. Prior to cell treatment, the $A\beta_{1-42}$ peptide was incubated at a final concentration of 5 μM in reduced-serum medium in the absence and presence of compounds **8** (1 μM) and **11** (1 μM), for 24 h at 37 °C, to induce Aβ aggregation. SH-Y5Y cells were seeded in 96-well plates (2×10^4/well) and treated the next day with the pre-aggregated $A\beta_{1-42}$ in the absence and presence of compounds **8** and **11**. After 48 h treatment, the cell viability was determined using the CellTiter 96 Aqueous One Solution Cell Proliferation Assay (Promega, Madison, WI, USA), in accordance with the manufacturer instructions. Absorbance was measured with an automatic microplate reader (Tecan Safire^2, Switzerland) at a wavelength of 492 nm. The data are presented as percentages of the DMSO control.

4.11.4. Measurement of reactive oxygen species

Intracellular ROS levels were determined by staining the cells with the dichlorofluorescein diacetate (DCFH-DA) probe (Sigma, St. Louis, MO, USA). SH-Y5Y cells were seeded in 96-well plates (2×10^4/well), and the next day they were stained with 10 μM DCFH-DA in pre-warmed phosphate-buffered saline for 20 min at 37 °C. The cells were then washed with phosphate-buffered saline and cultured in reduced-serum medium for 15 min at 37 °C. Then the cells were pretreated without (control) and with compounds **8** or **11** (5 μM) for 30 min, following treatment with H_2O_2 for an additional 90 min. The fluorescence intensity was measured at 485 nm excitation and 530 nm emission using a microplate reader (Tecan Safire^2, Switzerland). The data are presented relative to the DMSO control.

4.12. In-vitro permeability assay with Caco2 cells

Caco-2 cells were obtained from American Type Culture Collection (HTB.37), and were grown on Transwell Costar culture inserts with a polycarbonate membrane (diameter, 12 mm; pore size, 0.4 μm). Then 50,000 cells/filter membrane were used for seeding, and the medium was changed every 2 days. At day 20, the transepithelial electrical resistance (TEER) was measured for each filter with Caco-2 cell monolayers. If the TEER was in the range of 800–1100 cm^2, the Caco-2 cell monolayers were used for the subsequent testing of permeability at day 21. P-glycoprotein activity was confirmed with Rhodamine123.

Ringer buffer with 10 mM D-glucose or 10 mM mannitol on the apical and basolateral sides of the tissue, respectively, was used as the incubation saline. The tissue was kept at 37 °C in a carbogen (95% O_2, 5% CO_2) atmosphere. The addition of stock solutions of compounds **8**, **11** and fluorescein into the donor compartment provided the final 100 μM donor concentration for compounds **8** and **11**, and 20 μM for fluorescein. The stock solutions were added to either the apical or the basolateral compartment, to obtain bidirectional permeability measurements. Six samples were withdrawn in 20-min intervals. Here, 300 μL was taken from the 1500 μL basolateral acceptor compartment and 100 μL from the 500 μL apical acceptor compartment at each sampling time. These volumes were immediately replaced by the appropriate fresh incubation saline. The concentrations of compounds **8** and **11** in the samples were determined by HPLC-UV immediately after the experiment. The analysis was performed on an Agilent 1100 system (with degasser, binary pump, well plate sampler, column thermostat, diode-array detector) using a Zorbax Eclipse XDB-C18 column (4.6 × 75 mm, 3.5 μm) at 50 °C, with a mobile phase consisting of A (0.5% ammonium phosphate, pH 3.0) and B (MeCN) with a flow rate of 2.0 mL/min. For compound **8**, the A:B ratio in the mobile phase was 85:15, the detection wavelength was 246 nm, and the retention time was 1.71 min. For compound **11**, the A:B ratio in the mobile phase was 81.5:18.5, the detection wavelength was 252 nm, and the retention time was 1.61 min. The injection volume was 50 μL.

4.13. In-vitro blood-brain barrier permeation assay

To estimate the potential of compounds **8** and **11** to cross the BBB, PAMPA-BBBs were performed as described previously [70]. The PAMPA-BBB Explorer Test System was obtained from pION (pION Inc., MA, USA), and the assays were performed according to the manufacturer instructions. Briefly, the test compounds and the set of standard compounds were dissolved in DMSO at 10 mM. The stock DMSO solutions were further diluted in Prisma HT buffer, pH 7.40 (final concentration, 50 μM). The donor 96-well microplates were equipped with Sphere stirrers (stainless steel; diameter, 3.2 mm; Next Advance, USA), and filled with buffered solutions of the test compounds (180 μL per well) in quadruplicate. Each filter membrane on the 96-well acceptor plate was impregnated with 5 μL pION BBB-1 lipid solution. The acceptor plate was filled with Brain Sink buffer (200 μL per well) and placed on the donor plate. The plate 'sandwich' was then incubated for 16 h at room temperature without stirring. The plates were then carefully separated and the absorbance spectra of the blank (Prisma HT buffer, pH 7.40), donor, acceptor and reference wells were measured with a microplate reader (Synergy H4; BioTek Instruments, Inc., VT, USA). The logarithms of the effective permeability ($\log P_e$) were calculated using the PAMPA Explorer Software (pION Inc.).

Accession codes

Atomic coordinates and structure factors for the crystal structure of compound **11** in complex with hBChE have been deposited in the Protein Data Bank (PDB code 6F7Q). The authors will release the atomic coordinates upon publication.

Conflicts of interest

The authors declare that they have no competing financial interests.

Funding

This study was supported by the Slovenian Research Agency (project L1-8157 and bilateral project ARRS-CEA), the Agence Nationale de la Recherche (ANR-12-BS07-0008-03), the France-Alzheimer Foundation (FA-AAP-2013-65-101349), and Institut Francais (for one month scholarship granted to Damijan Knez).

Acknowledgements

We thank Andreja Pirnat and Nevenka Lilik for their contributions. We thank Dr. Dušan Žigon (Jožef Stefan Institute, Ljubljana, Slovenia) for performing the mass spectrometry measurements. We also thank Dr. Chris Berrie for critical reading of the manuscript.

Abbreviations

Aβ	amyloid β
ACh	acetycholine
AChE	acetylcholinesterase
AD	Alzheimer's disease
ADMET	absorption, distribution, metabolism, excretion and toxicity
BBB	blood-brain barrier
BChE	butyrylcholinesterase
Caco-2	heterogeneous human epithelial colorectal adenocarcinoma cells
CCA	coumarin-3-carboxylic acid
CDI	carbonyldiimidazole
ChE	cholinesterase
CNS	central nervous system
DCFH-DA	dichlorofluorescein diacetate
DMF	dimethylformamide
DMSO	dimethyl sulphoxide
DPPH	2,2-dipheny-l-1-picrylhydrazyl
HATU	1[bis(dimethylamino)methylene]-1*H*-1,2,3-triazolo [4,5-*b*]pyridinium 3-oxid hexafluorophosphate
hBChE	human butyrylcholinesterase
8-HQ	8-hydroxyquinoline
hAChE	human acetylcholinesterase
MTDL(s)	multi-target-directed ligand(s)
MTS	(3-(4,5-dimethylthiazol-2-yl)-5-(3-carboxymethoxyphenyl)-2-(4-sulfophenyl)-2*H*-tetrazolium, inner salt)
NMR	nuclear magnetic resonance
PAMPA	parallel artificial membrane permeation assay
ROS	reactive oxygen species
TBTU	*O* -(benzotriazol-1-yl)-*N*,*N*,*N*′,*N*′-tetramethyluronium tetrafluoroborate
TEER	transepithelial electrical resistance
TFA	2,2,2-trifluoroacetic acid
THF	tetrahydrofuran

Appendix A. Supplementary data

Supplementary data related to this article can be found at https://doi.org/10.1016/j.ejmech.2018.07.033

References

[1] M.J. Prince, A. Comas-Herrera, M. Knapp, M. Guerchet, M. Karagiannidou, World Alzheimer report 2016-Improving healthcare for people living with dementia, Alzheimer's Disease International (2016) 1–132.
[2] WHO, Dementia, 2018. http://www.who.int/news-room/fact-sheets/detail/dementia. (Accessed 9 June 2018).
[3] B. Winblad, P. Amouyel, S. Andrieu, C. Ballard, C. Brayne, H. Brodaty, A. Cedazo-Minguez, B. Dubois, D. Edvardsson, H. Feldman, L. Fratiglioni, G.B. Frisoni, S. Gauthier, J. Georges, C. Graff, K. Iqbal, F. Jessen, G. Johansson, L. Jonsson, M. Kivipelto, M. Knapp, F. Mangialasche, R. Melis, A. Nordberg, M.O. Rikkert, C. Qiu, T.P. Sakmar, P. Scheltens, L.S. Schneider, R. Sperling, L.O. Tjernberg, G. Waldemar, A. Wimo, H. Zetterberg, Defeating Alzheimer's disease and other dementias: a priority for European science and society, Lancet Neurol. 15 (2016) 455–532.
[4] A. Contestabile, The history of the cholinergic hypothesis, Behav. Brain Res. 221 (2011) 334–340.
[5] T.H. Ferreira-Vieira, I.M. Guimaraes, F.R. Silva, F.M. Ribeiro, Alzheimer's disease: targeting the cholinergic system, Curr. Neuropharmacol. 14 (2016) 101–115.
[6] J. Hartmann, C. Kiewert, E.G. Duysen, O. Lockridge, N.H. Greig, J. Klein, Excessive hippocampal acetylcholine levels in acetylcholinesterase-deficient mice are moderated by butyrylcholinesterase activity, J. Neurochem. 100 (2007) 1421–1429.
[7] E. Giacobini, Cholinesterases: new roles in brain function and in Alzheimer's disease, Neurochem. Res. 28 (2003) 515–522.
[8] A. Nordberg, C. Ballard, R. Bullock, T. Darreh-Shori, M. Somogyi, A review of butyrylcholinesterase as a therapeutic target in the treatment of Alzheimer's disease, Prim Care Companion CNS Disord 15 (2013).
[9] L. Blanco-Silvente, X. Castells, M. Saez, M.A. Barcelo, J. Garre-Olmo, J. Vilalta-Franch, D. Capella, Discontinuation, efficacy, and safety of cholinesterase inhibitors for Alzheimer's disease: a meta-analysis and meta-regression of 43 randomized clinical trials enrolling 16 106 patients, Int. J. Neuropsychopharmacol. 20 (2017) 519–528.
[10] M. Noetzli, C.B. Eap, Pharmacodynamic, pharmacokinetic and pharmacogenetic aspects of drugs used in the treatment of Alzheimer's disease, Clin. Pharmacokinet. 52 (2013) 225–241.
[11] N.H. Greig, T. Utsuki, D.K. Ingram, Y. Wang, G. Pepeu, C. Scali, Q.S. Yu, J. Mamczarz, H.W. Holloway, T. Giordano, D.M. Chen, K. Furukawa, K. Sambamurti, A. Brossi, D.K. Lahiri, Selective butyrylcholinesterase inhibition elevates brain acetylcholine, augments learning and lowers Alzheimer beta-amyloid peptide in rodent, P Natl Acad Sci USA 102 (2005) 17213–17218.
[12] Y. Furukawa-Hibi, T. Alkam, A. Nitta, A. Matsuyama, H. Mizoguchi, K. Suzuki, S. Moussaoui, Q.S. Yu, N.H. Greig, T. Nagai, K. Yamada, Butyrylcholinesterase inhibitors ameliorate cognitive dysfunction induced by amyloid-beta peptide in mice, Behav. Brain Res. 225 (2011) 222–229.
[13] Q. Li, H. Yang, Y. Chen, H. Sun, Recent progress in the identification of selective butyrylcholinesterase inhibitors for Alzheimer's disease, Eur. J. Med. Chem. 132 (2017) 294–309.
[14] U. Kosak, B. Brus, D. Knez, R. Sink, S. Zakelj, J. Trontelj, A. Pislar, J. Slenc, M. Gobec, M. Zivin, L. Tratnjek, M. Perse, K. Salat, A. Podkowa, B. Filipek, F. Nachon, X. Brazzolotto, A. Wieckowska, B. Malawska, J. Stojan, I.M. Rascan, J. Kos, N. Coquelle, J.P. Colletier, S. Gobec, Development of an in-vivo active reversible butyrylcholinesterase inhibitor, Sci. Rep. 6 (2016) 39495.
[15] U. Kosak, B. Brus, D. Knez, S. Zakelj, J. Trontelj, A. Pislar, R. Sink, M. Jukic, M. Zivin, A. Podkowa, F. Nachon, X. Brazzolotto, J. Stojan, J. Kos, N. Coquelle, K. Salat, J.P. Colletier, S. Gobec, The magic of crystal dtructure-based inhibitor optimization: development of a butyrylcholinesterase inhibitor with picomolar affinity and in vivo activity, J. Med. Chem. 61 (2018) 119–139.
[16] G. Mushtaq, N.H. Greig, J.A. Khan, M.A. Kamal, Status of acetylcholinesterase and butyrylcholinesterase in Alzheimer's disease and type 2 diabetes mellitus, CNS Neurol. Disord. - Drug Targets 13 (2014) 1432–1439.
[17] A. Gella, N. Durany, Oxidative stress in Alzheimer disease, Cell Adhes. Migrat. 3 (2009) 88–93.
[18] T. Jiang, Q. Sun, S. Chen, Oxidative stress: a major pathogenesis and potential therapeutic target of antioxidative agents in Parkinson's disease and Alzheimer's disease, prog, Neurobiology (Cph.) 147 (2016) 1–19.
[19] M.G. Savelieff, S. Lee, Y. Liu, M.H. Lim, Untangling amyloid-beta, tau, and metals in Alzheimer's disease, ACS Chem. Biol. 8 (2013) 856–865.
[20] R.J. O'Brien, P.C. Wong, Amyloid precursor protein processing and Alzheimer's disease, Annu. Rev. Neurosci. 34 (2011) 185–204.
[21] T. Mohamed, A. Shakeri, P.P. Rao, Amyloid cascade in Alzheimer's disease: recent advances in medicinal chemistry, Eur. J. Med. Chem. 113 (2016) 258–272.
[22] K.P. Kepp, Alzheimer's disease due to loss of function: a new synthesis of the available data, Prog. Neurobiol. 143 (2016) 36–60.
[23] M. Rosini, E. Simoni, A. Milelli, A. Minarini, C. Melchiorre, Oxidative stress in Alzheimer's disease: are we connecting the dots? J. Med. Chem. 57 (2014) 2821–2831.
[24] S. Ayton, P. Lei, A.I. Bush, Metallostasis in Alzheimer's disease, Free Radic. Biol. Med. 62 (2013) 76–89.
[25] C. Cheignon, M. Tomas, D. Bonnefont-Rousselot, P. Faller, C. Hureau, F. Collin, Oxidative stress and the amyloid beta peptide in Alzheimer's disease, Redox Biol 14 (2018) 450–464.
[26] F. Collin, C. Cheignon, C. Hureau, Oxidative stress as a biomarker for Alzheimer's disease, Biomarkers Med. (2018), https://doi.org/10.2217/bmm-2017-0456.
[27] P. Bawa, P. Pradeep, P. Kumar, Y.E. Choonara, G. Modi, V. Pillay, Multi-target therapeutics for neuropsychiatric and neurodegenerative disorders, Drug Discov. Today 21 (2016) 1886–1914.
[28] M. de Freitas Silva, K.S.T. Dias, V.S. Gontijo, C.J.C. Ortiz, C. Viega, Multi-target directed drugs as a modern approach for drug design towards Alzheimer's

disease: an update, Curr. Med. Chem. (2018), https://doi.org/10.2174/0929867325666180111101843.
[29] S. Das, S. Basu, Multi-targeting strategies for Alzheimer's disease therapeutics: pros and cons, Curr. Top. Med. Chem. 17 (2017) 3017–3061.
[30] L. Ismaili, B. Refouvelet, M. Benchekroun, S. Brogi, M. Brindisi, S. Gemma, G. Campiani, S. Filipic, D. Agbaba, G. Esteban, M. Unzeta, K. Nikolic, S. Butini, J. Marco-Contelles, Multitarget compounds bearing tacrine- and donepezil-like structural and functional motifs for the potential treatment of Alzheimer's disease, Prog. Neurobiol. 151 (2017) 4–34.
[31] R. Leon, A.G. Garcia, J. Marco-Contelles, Recent advances in the multitarget-directed ligands approach for the treatment of Alzheimer's disease, Med. Res. Rev. 33 (2013) 139–189.
[32] R.E. Hughes, K. Nikolic, R.R. Ramsay, One for all? Hitting multiple Alzheimer's disease targets with one drug, Front. Neurosci. 10 (2016) 177.
[33] R.R. Ramsay, M. Majekova, M. Medina, M. Valoti, Key targets for multi-target ligands designed to combat neurodegeneration, Front. Neurosci. 10 (2016) 375.
[34] D. Dolles, M. Hoffmann, S. Gunesch, O. Marinelli, J. Moller, G. Santoni, A. Chatonnet, M.J. Lohse, H.J. Wittmann, A. Strasser, M. Nabissi, T. Maurice, M. Decker, Structure-activity relationships and computational investigations into the development of potent and balanced dual-acting butyrylcholinesterase inhibitors and human cannabinoid receptor 2 ligands with pro-cognitive in vivo profiles, J. Med. Chem. 61 (2018) 1646–1663.
[35] R. Morphy, Z. Rankovic, Designed multiple ligands. An emerging drug discovery paradigm, J. Med. Chem. 48 (2005) 6523–6543.
[36] M. Singh, M. Kaur, N. Chadha, O. Silakari, Hybrids: a new paradigm to treat Alzheimer's disease, Mol. Divers. 20 (2016) 271–297.
[37] D. Knez, B. Brus, N. Coquelle, I. Sosic, R. Sink, X. Brazzolotto, J. Mravljak, J.P. Colletier, S. Gobec, Structure-based development of nitroxoline derivatives as potential multifunctional anti-Alzheimer agents, Bioorg. Med. Chem. 23 (2015) 4442–4452.
[38] C.A. Kontogiorgis, Y. Xu, D. Hadjipavlou-Litina, Y. Luo, Coumarin derivatives protection against ROS production in cellular models of Abeta toxicities, Free Radic. Res. 41 (2007) 1168–1180.
[39] J.A. Jacobsen, J.L. Fullagar, M.T. Miller, S.M. Cohen, Identifying chelators for metalloprotein inhibitors using a fragment-based approach, J. Med. Chem. 54 (2011) 591–602.
[40] V. Oliveri, G. Vecchio, 8-Hydroxyquinolines in medicinal chemistry: a structural perspective, Eur. J. Med. Chem. 120 (2016) 252–274.
[41] M. Sova, Antioxidant and antimicrobial activities of cinnamic acid derivatives, Mini Rev. Med. Chem. 12 (2012) 749–767.
[42] Z. Rankovic, CNS drug design: balancing physicochemical properties for optimal brain exposure, J. Med. Chem. 58 (2015) 2584–2608.
[43] L. Lannfelt, K. Blennow, H. Zetterberg, Safety, efficacy, and biomarker findings of PBT2 in targeting A beta as a modifying therapy for Alzheimer's disease: a phase IIa, double-blind, randomised, placebo-controlled trial (vol 7, pg 779, 2008), Lancet Neurol. 8 (2009) 981, 981.
[44] L.S. Schneider, F. Mangialasche, N. Andreasen, H. Feldman, E. Giacobini, R. Jones, V. Mantua, P. Mecocci, L. Pani, B. Winblad, M. Kivipelto, Clinical trials and late-stage drug development for Alzheimer's disease: an appraisal from 1984 to 2014, J. Intern. Med. 275 (2014) 251–283.
[45] U. Kosak, B. Brus, S. Gobec, Straightforward synthesis of orthogonally protected piperidin-3-ylmethanamine and piperidin-4-ylmethanamine derivatives, Tetrahedron Lett. 55 (2014) 2037–2039.
[46] I. Sosic, A. Mitrovic, H. Curic, D. Knez, H. Brodnik Zugelj, B. Stefane, J. Kos, S. Gobec, Cathepsin B inhibitors: further exploration of the nitroxoline core, Bioorg. Med. Chem. Lett 28 (2018) 1239–1247.
[47] C.A. Lipinski, F. Lombardo, B.W. Dominy, P.J. Feeney, Experimental and computational approaches to estimate solubility and permeability in drug discovery and development settings, Adv. Drug Deliv. Rev. 46 (2001) 3–26.
[48] H. van de Waterbeemd, G. Camenisch, G. Folkers, J.R. Chretien, O.A. Raevsky, Estimation of blood-brain barrier crossing of drugs using molecular size and shape, and H-bonding descriptors, J. Drug Target. 6 (1998) 151–165.
[49] A.K. Ghose, T. Herbertz, R.L. Hudkins, B.D. Dorsey, J.P. Mallamo, Knowledge-Based, Central Nervous System (CNS) Lead selection and lead optimization for CNS drug discovery, ACS Chem. Neurosci. 3 (2012) 50–68.
[50] J.D. Irvine, L. Takahashi, K. Lockhart, J. Cheong, J.W. Tolan, H.E. Selick, J.R. Grove, MDCK (Madin-Darby canine kidney) cells: a tool for membrane permeability screening, J. Pharmacol. Sci. 88 (1999) 28–33.
[51] B. Brus, U. Kosak, S. Turk, A. Pislar, N. Coquelle, J. Kos, J. Stojan, J.P. Colletier, S. Gobec, Discovery, biological evaluation, and crystal structure of a novel nanomolar selective butyrylcholinesterase inhibitor, J. Med. Chem. 57 (2014) 8167–8179.
[52] O.P. Sharma, T.K. Bhat, DPPH antioxidant assay revisited, Food Chem. 113 (2009) 1202–1205.
[53] G. Eskici, P.H. Axelsen, Copper and oxidative stress in the pathogenesis of Alzheimer's disease, Biochemistry 51 (2012) 6289–6311.
[54] F. Hane, Z. Leonenko, Effect of metals on kinetic pathways of amyloid-beta aggregation, Biomolecules 4 (2014) 101–116.
[55] S.S. Hindo, A.M. Mancino, J.J. Braymer, Y.H. Liu, S. Vivekanandan, A. Ramamoorthy, M.H. Lim, Small molecule modulators of copper-induced A beta aggregation, J. Am. Chem. Soc. 131 (2009) 16663–16665.
[56] P.J. Crouch, K.J. Barnham, Therapeutic Redistribution of metal ions to treat Alzheimer's disease, Accounts Chem. Res. 45 (2012) 1604–1611.
[57] E. Ferrada, V. Arancibia, B. Loeb, E. Norambuena, C. Olea-Azar, J.P. Huidobro-Toro, Stoichiometry and conditional stability constants of Cu(II) or Zn(II) clioquinol complexes; implications for Alzheimer's and Huntington's disease therapy, Neurotoxicology 28 (2007) 445–449.
[58] C. Sgarlata, G. Arena, R.P. Bonomo, A. Giuffrida, G. Tabbi, Simple and mixed complexes of copper(II) with 8-hydroxyquinoline derivatives and amino acids: characterization in solution and potential biological implications, J. Inorg. Biochem. 180 (2018) 89–100.
[59] M. Patel, Targeting oxidative stress in central nervous system disorders, Trends Pharmacol. Sci. 37 (2016) 768–778.
[60] K.M. Lincoln, T.E. Richardson, L. Rutter, P. Gonzalez, J.W. Simpkins, K.N. Green, An N-heterocyclic amine chelate capable of antioxidant capacity and amyloid disaggregation, ACS Chem. Neurosci. 3 (2012) 919–927.
[61] M.R. Jones, E. Mathieu, C. Dyrager, S. Faissner, Z. Vaillancourt, K.J. Korshavn, M.H. Lim, A. Ramamoorthy, V. Wee Yong, S. Tsutsui, P.K. Stys, T. Storr, Multi-target-directed phenol-triazole ligands as therapeutic agents for Alzheimer's disease, Chem. Sci. 8 (2017) 5636–5643.
[62] I.O. Zakharova, T.V. Sokolova, Y.A. Vlasova, L.V. Bayunova, M.P. Rychkova, N.F. Avrova, Alpha-tocopherol at nanomolar concentration protects cortical neurons against oxidative stress, Int. J. Mol. Sci. 18 (2017).
[63] N.E. Craft, T.B. Haitema, K.M. Garnett, K.A. Fitch, C.K. Dorey, Carotenoid, tocopherol, and retinol concentrations in elderly human brain, J. Nutr. Health Aging 8 (2004) 156–162.
[64] D. Mechlovich, T. Amit, S.A. Mandel, O. Bar-Am, K. Bloch, P. Vardi, M.B. Youdim, The novel multifunctional, iron-chelating drugs M30 and HLA20 protect pancreatic beta-cell lines from oxidative stress damage, J. Pharmacol. Exp. Therapeut. 333 (2010) 874–882.
[65] A. Avdeef, Absorption and Drug Development : Solubility, Permeability, and Charge State, second ed., John Wiley & Sons, Hoboken, N.J, 2012.
[66] L. Di, E.H. Kerns, Transporter methods, in: Drug–like Properties: Concepts, Structure, Design, and Methods from ADME to Toxicity Optimization, Academic Press, 2016, pp. 339–350.
[67] S. Zakelj, K. Berginc, R. Roskar, B. Kraljic, A. Kristl, Do the recommended standards for in vitro biopharmaceutic classification of drug permeability meet the "passive transport" criterion for biowaivers? Curr. Drug Metabol. 14 (2013) 21–27.
[68] S.G. Summerfield, A.J. Stevens, L. Cutler, M. del Carmen Osuna, B. Hammond, S.P. Tang, A. Hersey, D.J. Spalding, P. Jeffrey, Improving the in vitro prediction of in vivo central nervous system penetration: integrating permeability, P-glycoprotein efflux, and free fractions in blood and brain, J. Pharmacol. Exp. Therapeut. 316 (2006) 1282–1290.
[69] E.L. Eliel, D. Kandasamy, C.Y. Yen, K.D. Hargrave, Conformational-Analysis .39. C-13 NMR-spectra of saturated heterocycles. 9. piperidine and *N*-methylpiperidine, J. Am. Chem. Soc. 102 (1980) 3698–3707.
[70] U. Kosak, D. Knez, N. Coquelle, B. Brus, A. Pislar, F. Nachon, X. Brazzolotto, J. Kos, J.P. Colletier, S. Gobec, N-Propargylpiperidines with naphthalene-2-carboxamide or naphthalene-2-sulfonamide moieties: potential multifunctional anti-Alzheimer's agents, Bioorg. Med. Chem. 25 (2017) 633–645.
[71] X. Brazzolotto, M. Wandhammer, C. Ronco, M. Trovaslet, L. Jean, O. Lockridge, P.Y. Renard, F. Nachon, Human butyrylcholinesterase produced in insect cells: huprine-based affinity purification and crystal structure, FEBS J. 279 (2012) 2905–2916.
[72] F. Mao, J. Yan, J. Li, X. Jia, H. Miao, Y. Sun, L. Huang, X. Li, New multi-target-directed small molecules against Alzheimer's disease: a combination of resveratrol and clioquinol, Org. Biomol. Chem. 12 (2014) 5936–5944.